Earth, Planets and Space

FULL PAPER

Open Access

Preliminary study on hydrological angular momentum determined from CMIP6 historical simulations

Jolanta Nastula[1], Justyna Śliwińska[1*], Tomasz Kur[1], Małgorzata Wińska[2] and Aleksander Partyka[1]

Abstract

Polar motion (PM) is an essential parameter needed to transform coordinates between celestial and terrestrial reference frames, thus playing a crucial role in precise positioning and navigation. The role of hydrological signals in PM excitation is not yet fully understood, which is largely because of the lack of agreement between estimates of hydrological angular momentum (HAM) computed from different data sources. In this study, we used data obtained from the latest, sixth phase of the Coupled Model Intercomparison Project (CMIP6) to assess the impact of the continental hydrosphere on PM excitation. To do so, we exploited soil moisture and snow water variables obtained from historical simulations of CMIP6 to estimate climate-based HAM. The HAM series were computed, then we analysed their variability in terms of trends, seasonal and non-seasonal oscillations. An important part of this study is the validation of HAM estimates based on comparison with the hydrological signal in geodetically observed PM excitation (geodetic residuals, GAO). In addition, HAM series based on climate models were compared with those determined from global gravimetric data provided by the Gravity Recovery and Climate Experiment (GRACE) mission, and from the Land Surface Discharge Model (LSDM). This study also aimed to identify the most appropriate CMIP6 models for interpretation of PM variations. Overall, the correspondence between GAO and HAM received from CMIP6 was lower than the previously obtained consistency with GRACE results, and the level of agreement was dependent on the oscillation considered and the model used. However, it may be possible to identify several CMIP6 models from among the almost 100 available that provides a HAM series more compatible with GAO than HAM from GRACE or LSDM, especially in annual oscillations. The GISS-E2-1-G_historical_r10i1p1f1 model was found to provide the highest consistency with GAO for annual prograde amplitudes, GFDL-CM4_historical_r1i1p1f1 for annual retrograde amplitudes, BCC-ESM1_historical_r3i1p1f1 for the annual prograde phase, and MIROC-ES2L_historical_r2i1p1f2 for the annual retrograde phase. Because of their length, the CMIP6 data allow for analysis of the past and future changes in HAM from 1850 to 2100, which is of particular importance in the exploration of the impact of climate change on PM excitation.

Keywords: CMIP6, GRACE, Climate, Polar motion, Hydrosphere, LSDM

*Correspondence: jsliwinska@cbk.waw.pl

[1] Centrum Badań Kosmicznych Polskiej Akademii Nauk, Bartycka 18A, 00-716 Warsaw, Poland
Full list of author information is available at the end of the article

Graphical Abstract

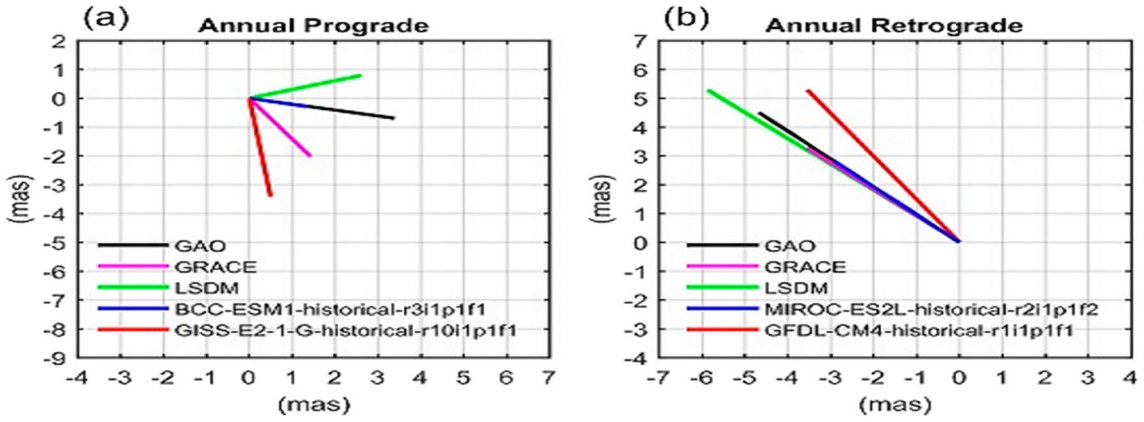

Introduction

The Earth is a dynamic and complex system with a continually changing global mass distribution of the atmosphere, ocean, land hydrosphere, and cryosphere. These mass redistributions, along with the movements of the solid part of the Earth, such as tectonic plates movements or earthquakes, cause changes in Earth's rotation. The motion of the rotation axis of the Earth with respect to its surface is defined as the polar motion (PM) and is represented by the two coordinates, x_P and y_P, pointing along the longitudes of mean Greenwich and 90 °E, respectively. Information on PM variations obtained from geodetic observations and geophysical models provide an integrated view of Earth system changes.

The conservation law of angular momentum in the Earth's equatorial plane governs PM in the absence of external torques. This relationship is described by the Liouville equations. After introducing the excitation functions and their linearization, the angular momentum balance law can be expressed in the terrestrial reference frame (Munk and MacDonald 1960). Barnes et al. (1983) and Brzeziński (1992) modified linearized Liouville equations provided by Munk and MacDonald (1960) by introducing effective angular momentum (EAM) functions, expressed as two equatorial components (χ_1, χ_2) and one axial component (χ_3), which have a geophysical interpretation and can be derived from observational data. The χ_1 and χ_2 components of the EAM functions describe PM excitation caused by perturbing forces, while χ_3 is related to length-of-day variations induced by these forces. Depending on the disturbing factor, we can distinguish the atmospheric, oceanic, and hydrological EAM function, also known as the atmospheric angular momentum (AAM), oceanic angular momentum (OAM), and hydrological angular momentum (HAM), respectively.

PM changes are mostly composed of two counterclockwise wobbles at periods of 433 days (Chandler wobble) and 365 days (annual wobble). Annual and interannual PM variations are forced by the relative motion of winds and ocean currents and the mass redistribution of air and water (Gross 2007, 2015). The major part of PM changes are explained by the atmosphere (both winds and surface pressure) (e.g. Barnes et al. 1983; Chao and Au 1991; Gross 2003) and by the oceans (both ocean bottom pressure and currents) (Wahr 1983; Dickey et al. 1993; Ponte et al. 1998; Gross 2003). However, results from the analysis of different sources of land hydrological signals in PM excitation, including global models and satellite data, suggest that HAM may explain some part of the PM excitation changes remaining after removing AAM and OAM effects (Chen and Wilson 2005; Jin et al. 2010; Seoane et al. 2011; Wińska 2016; Wińska et al. 2016; Śliwińska et al. 2019).

HAM can be estimated from global models of the continental hydrosphere, measurements of Earth's gravity field variations, and climate models. Hydrological models have been processed by many institutes using satellite and terrestrial observations as well as simulations of the spatial and temporal distribution of terrestrial water storage (TWS) components such as soil moisture, water in reservoirs, groundwater, snow, ice, and water in biomass. It has been shown, however, that HAM estimates determined from different hydrological models do not

agree well with each other (Brzeziński et al. 2009; Chen and Wilson 2005; Chen et al. 2000; Nastula et al. 2011, 2019; Wińska et al. 2016, 2017). Studies of the impact of land hydrosphere on PM excitation determined from TWS distribution have produced inconsistent results, with considerable variation in amplitudes and phases at seasonal timescales (Nastula et al. 2011; Chen and Wilson 2005; Wińska et al. 2016; Śliwińska et al. 2019). Such inconsistencies might result from the fact that TWS has not been adequately measured at the continental scale (Lettenmaier and Famiglietti 2006). This is mainly due to the lack of a full global network for regular TWS monitoring. While ground- and microwave satellite-based techniques can measure some individual components such as soil moisture (Njoku et al. 2003) and surface water (Alsdorf and Lettenmaier 2003), there have been no integrated measurements of TWS.

Climate models are more complex than hydrological ones, because, apart from land hydrosphere components, they also deliver parameters essential to study atmosphere, oceans, and cryosphere (Taylor et al. 2012). A large number of climate models are stored and made available to the users in the frame of the Coupled Model Intercomparison Project (CMIP). The newest release of this initiative, CMIP Phase 6 (CMIP6), represents a substantial expansion over its previous version, CMIP5, in terms of the number of modelling groups participating in the project, the number of models registered, the number of future scenarios examined, and the number of different experiments conducted (Eyring et al. 2016). However, CMIP6 models are subject to the same limitations as hydrological models. They do not provide the full information on all TWS components, in particular there is a lack of groundwater storage and ice mass changes in the polar regions for these models. In addition, the models provide information on soil moisture only up to the depth specified by the model.

The launch of the Gravity Recovery and Climate Experiment (GRACE) mission and its successor, GRACE Follow-On (GRACE-FO), resolved the lack of direct observations of large scale TWS estimates. The missions' measurements are a new source of data for studying the Earth's time-variable gravity field variations, which can be also exploited to investigate the hydrological part of PM excitation changes (Landerer et al. 2020; Tapley et al. 2004). Since the launch of the GRACE mission in 2002, the GRACE science teams at the Center for Space Research (CSR, Austin, USA), GeoForschungsZentrum (GFZ, Potsdam, Germany), and the Jet Propulsion Laboratory (JPL, Pasadena, USA) regularly provide GRACE-based monthly gravity field solutions. GRACE measurements provide comprehensive information on total TWS variations including all of their components. The data can therefore be used to quantify the water storage part in the hydrological balance equation, which is especially useful for evaluating hydrological budgets obtained from models (Tapley et al. 2004; Wahr et al. 2004). In recent years, data from GRACE and GRACE-FO have been applied to interpret PM excitation disturbances, focusing on various oscillations and different time periods (Brzeziński et al. 2009; Göttl et al. 2018; Jin et al. 2010; Seoane et al. 2009, 2012; Śliwińska et al. 2020a, b, 2021a, b). It has also been shown that the use of gravimetric data from GRACE can lead to a higher consistency between HAM and geodetically observed hydrological signal in PM excitation compared with exploiting geophysical models of the hydrosphere (Nastula et al. 2019; Śliwińska et al. 2020a; Wińska et al. 2017). However, despite their unprecedented advantages, GRACE and GRACE-FO suffer from some limitations. In particular, there is a one-year data gap between the end of the GRACE operation and beginning of the GRACE-FO measurements, forcing researchers to seek other sources of uninterrupted data on TWS variation. In addition, studies of the impact of climate change on HAM, which is currently of interest to many scientists, require much longer datasets on TWS changes. However, GRACE and GRACE-FO measurements are available only for the period from 2002 to the present. So far, the only global data on changes in TWS components, which covers both their past evolution and future changes, are the CMIP6 models. The models provide data needed for HAM analysis from 1850 up to 2100, which is sufficient time to assess the impact of climate change on HAM.

The main objective of the current study was to check whether the latest climate models provide realistic data to determine HAM. To achieve this, we used the climate models collected and made available as a part of CMIP6. We conducted a detailed analysis from a total of 99 CMIP6 historical models and tested their usefulness for studying PM variations induced by the continental hydrosphere to identify the most appropriate climate models for HAM determination. Moreover, we assessed the quality of computed CMIP6-based HAM in various spectral bands and compared them with hydrological signal in geodetically observed PM excitation called geodetic residuals (GAO). In addition, HAM based on climate models were also compared with HAM determined from global gravimetric data provided by GRACE, and HAM obtained from the LSDM (Land Surface Discharge Model). The application of climate models in exploring the temporal behaviour of the hydrological signal in PM excitation changes is essential to improve understanding of the climate-related

mass redistribution caused by global warming. The CMIP6 models selected in this study, based on evaluation by comparison with GAO for the period 2003–2014, can be further used to analyse the past and future changes in the excitation of PM induced by the continental hydrosphere during periods for which observational data are not available.

Data and data processing

CMIP6 climate models

The sum of soil moisture and snow water was used to estimate the TWS from monthly CMIP6 models since these are the only TWS components provided in the CMIP6 archive that are needed for HAM computation. Other models, such as those from global land data assimilation system (GLDAS), also provide an estimate of the water in biomass; however, Śliwińska et al. (2019) showed that this variable only marginally affects HAM. We use snow water equivalent ('snw', mass of surface snow on the land portion of the grid cell divided by the land area in the grid cell; excludes snow on vegetation canopy or on sea ice) and soil water storage ('mrso', which are used in the CMIP6 archives and included water in all phases for all the soil layers) variables from CMIP6 to represent the TWS.

Depending on the model within CMIP6, a single variable is given either in one file or in several separate files that have different time intervals. For the purpose of this study, the variables given in a few separate files were merged into one in order to obtain one long time series for each of the variables. Models that showed visible jumps after this merge were excluded from further processing. Models that ended before 2013 were also removed from the analysis. We focused our analysis between 2003 and 2014, which is the period of GRACE activity excluding the initial and terminal phases of GRACE activity that had limited CMIP6 data availability. This selection led to the inclusion of 99 historical models out of several hundred (see Tables 8 and 9 in Appendix). The selected models have different spatial resolution (Table 8) and thus we started our analysis from the interpolation of the TWS fields into regular $1^\circ \times 1^\circ$ grids. Table 9 lists all 99 models used in our study.

GRACE data

In this study, we applied the sixth release (RL06) of GRACE Level-3 data in the form of TWS anomalies provided by CSR (CSR RL06 solution). The GRACE Level-3 processing performed by CSR included filtering with a 300-km Gaussian filter and the following corrections: removal of atmosphere and ocean impact through implementation of atmosphere and ocean dealiasing (AOD) data, removal of the impact of post-glacial rebound by applying a glacial isostatic adjustment (GIA) model, replacement of the C_{20} spherical harmonic (SH) coefficient with the more accurate estimate provided by the satellite laser ranging (SLR) technique, addition of degree-1 SH coefficients (not measured by GRACE), and truncation of SH coefficients at degree 60 (Bettadpur 2018).

There are several other GRACE Level-3 solutions processed by other centres (i.e. JPL and GFZ) and there are some differences between these solutions (Göttl et al. 2015, 2018; Meyrath and van Dam 2016; Nastula et al. 2019; Seoane et al. 2009; Śliwińska et al. 2020b). The main sources of discrepancies between GRACE data provided by various institutes are likely to be different background models applied (e.g. mean gravity field model, pole tides model, ocean tides model, solid Earth tides model, AOD data), data processing methods and parametrization schemes of accelerometer measurements and K-band ranging. There are also notable outliers in GRACE data like errors related to the polar orbit of satellites that induce vertical stripes on the TWS maps; effects of applying smoothing filters, which on the one hand, eliminate vertical stripes but on the other hand degrade part of the actual geophysical signal; leakage errors, signal attenuation resulting from limitation to the specified degree and order in spherical harmonic expression of geopotential; incomplete removal of some geophysical signals from GRACE gravity fields with the use of background models; difficulties of separation individual signals, especially the cryospheric one (Göttl et al. 2015, 2018; Chen 2019; Chen et al. 2021, 2022). Despite these outliers, GRACE measurements are an invaluable source of data that can be used to determine HAM.

Because this paper focuses on the preliminary analysis of usefulness of CMIP6 for HAM determination, we decided to exploit one GRACE temporal gravity field model for comparison with the results obtained from CMIP6. In this study, we considered the Level-3 GRACE CSR RL06 solution, because this has been shown to have the best agreement between HAM and GAO at seasonal and non-seasonal time scales (Śliwińska et al. 2020b, 2021a).

Hydrological model

For the analysis of HAM in the current study, in addition to CMIP6 and GRACE data, we also used the LSDM (Dill et al. 2009), which is forced with precipitation, evaporation, and temperature data from the European Centre for Medium-Range Weather Forecasts (ECMWF) atmospheric model. Among the hydrological models tested

to date for their usefulness of HAM determination, the LSDM provided the highest consistency between HAM and GAO (Nastula et al. 2019). The LSDM simulates global water storage variations in TWS components such as surface water (water in rivers, lakes, and wetlands), groundwater (only shallow layer), soil moisture, and water stored as snow and ice (without information about long-term ice mass changes) (Dill 2008). The LSDM also provides estimates of continental water flow velocities in rivers and aquifers, thus continental motion terms were calculated in addition to the mass term contributions from TWS variations (Dobslaw et al. 2010).

In this study, we applied daily HAM time series, calculated by GFZ from LSDM consistent with the GRACE de-aliasing products AOD1B RL06 (Atmosphere and Ocean Dealiasing Level-1b Release 6), which are publicly available at the GFZ website (http://rz-vm115.gfz-potsdam.de:8080/repository).

Geodetic residuals

The typical approach for evaluating HAM series is to compare them with GAO, which are the differences between geodetic angular momentum (GAM) obtained from precisely measured pole coordinates and the sum of AAM and OAM derived from geophysical models as follows (e.g. Jin et al. 2010; Seoane et al. 2011; Śliwińska et al. 2019; Wińska and Śliwińska 2019; Nastula et al. 2019; Nastula and Śliwińska 2020):

$$\mathrm{GAO} = \mathrm{GAM} - \mathrm{AAM} - \mathrm{OAM}. \tag{1}$$

The GAO series reflect the hydrological signal in geodetically observed PM. However, the GAO themselves can be affected by errors or uncertainties in observations of PM and models of AAM and OAM.

The relation between (χ_1, χ_2) components of GAM and (x_P, y_P) coordinates of the pole was described by the following equations (Brzeziński 1992; Eubanks 1993):

$$\chi(t) = \chi_1(t) + i\chi_2(t) = p(t) + \frac{i}{\sigma_c}\frac{\mathrm{d}p(t)}{\mathrm{d}t}, \tag{2}$$

$$p(t) = x_P(t) - i \cdot y_P(t), \tag{3}$$

where t is time and $\sigma_\mathrm{c} = 2\pi(1 + i/2Q)/T_\mathrm{c}$ is the complex Chandler frequency with Chandler period $T_\mathrm{c} = 433$ days and with a damping $Q = 100$ (Vicente and Wilson 2002).

The definition of χ_1 (along Greenwich Meridian) and χ_2 (along 90 °E meridian) components of GAM is not based on geophysical factors but on traditional assumptions. This definition makes χ_2 of GAM more sensitive to changes in mass over lands, especially in the Northern Hemisphere, while χ_1 is more responsive to changes over the oceans and ice cover. As a result, χ_2 of HAM tends to be better correlated with GAO for χ_2 than for χ_1.

The observations of pole coordinates needed for computation of GAM are available at daily intervals for the period 1962 to the present and are provided by International Earth Orientation and Reference Systems Service (IERS). The newest release of this series is Earth Orientation Parameters 14 Combined 04 (EOP 14 C04) solution based on combination of observations from SLR, Global Navigation Satellite Systems (GNSS), and very long baseline interferometry (VLBI).

AAM and OAM are usually determined using geophysical models of the atmosphere and ocean. In this study, GAO series were determined from two different combinations of compatible AAM and OAM models, where the sum of the masses in the atmosphere and ocean circulation is constant. First combination (GAO1) was calculated with the use of the National Centers for Environmental Prediction/National Center for Atmospheric Research (NCEP/NCAR) (Kalnay et al. 1996) (for AAM) and estimating the circulation and climate of the ocean (ECCO) (Fukumori et al. 2017) (for OAM). The second combination (GAO2) was calculated from the ECMWF model (for AAM) (Dobslaw et al. 2010) and the Max Planck Institute Ocean Model (MPIOM) (Jungclaus et al. 2013) (for OAM). All AAM and OAM series computed from those models are provided by IERS.

In our study, the mean value of the GAO1 and GAO2 was used as the reference GAO time series, which was compared with the HAM series calculated from different climate models, from LSDM, and from GRACE data.

Time series processing

Equatorial components (χ_1, χ_2) of HAM were computed from TWS distribution using the following equations (Barnes et al. 1983; Eubanks 1993):

$$\chi_1 = -\frac{1.0966R_\mathrm{e}^2}{C-A}\iint TWS(\varphi,\lambda,t)\sin\varphi\cos\varphi\cos\lambda\,\mathrm{d}S, \tag{4}$$

$$\chi_2 = -\frac{1.0966R_\mathrm{e}^2}{C-A}\iint TWS(\varphi,\lambda,t)\sin\varphi\cos\varphi\sin\lambda\,\mathrm{d}S, \tag{5}$$

where C and A are Earth's principal moments of inertia; R_e is the Earth's mean radius; (φ, λ, t) are latitude, longitude, and time, respectively; and $\mathrm{d}S$ is the surface area. For GRACE data, TWS anomalies were taken directly from the CSR RL06 solution, whereas for CMIP6 data, the TWS variations were computed as a sum of soil moisture and snow water.

In order to study the agreement between GAO and different HAM estimates, all time series were interpolated to the same time period (between 2003 and 2014) and filtered using a Gaussian filter to remove oscillations with frequencies higher than monthly. We decomposed the total signal of each time series into linear trends and seasonal and non-seasonal oscillations and analysed the contribution of each component separately.

To determine seasonal oscillations in GAO and for each HAM series, we used the least-squares method to fit a model comprising the second order polynomial and a sum of complex sinusoids with periods of 365.25 and 180.0 days (Brzeziński 1992; Brzeziński et al. 2009). A more detailed analysis of seasonal oscillations also included separation of seasonal series into prograde and retrograde circular terms for annual and semiannual variations. This approach allows thorough investigation of the amplitudes and phases of the seasonal oscillation. This method of analysing seasonal variations in PM excitation has been widely used in previous research (Brzeziński et al. 2009; Dobslaw et al. 2010; Seoane et al. 2011; Wińska et al. 2016).

The seasonal oscillations and trend in HAM and GAO are discussed here, as they are dominant in PM excitation. However, the influence of HAM on PM excitation in other spectral bands is non-negligible. The non-seasonal oscillations of various HAM and GAO series were computed after removing the fitted seasonal oscillations and linear trends from original interpolated and filtered time series. The non-seasonal series contain all oscillations other than the trends and seasonal changes, with periods ranging from several months to several years.

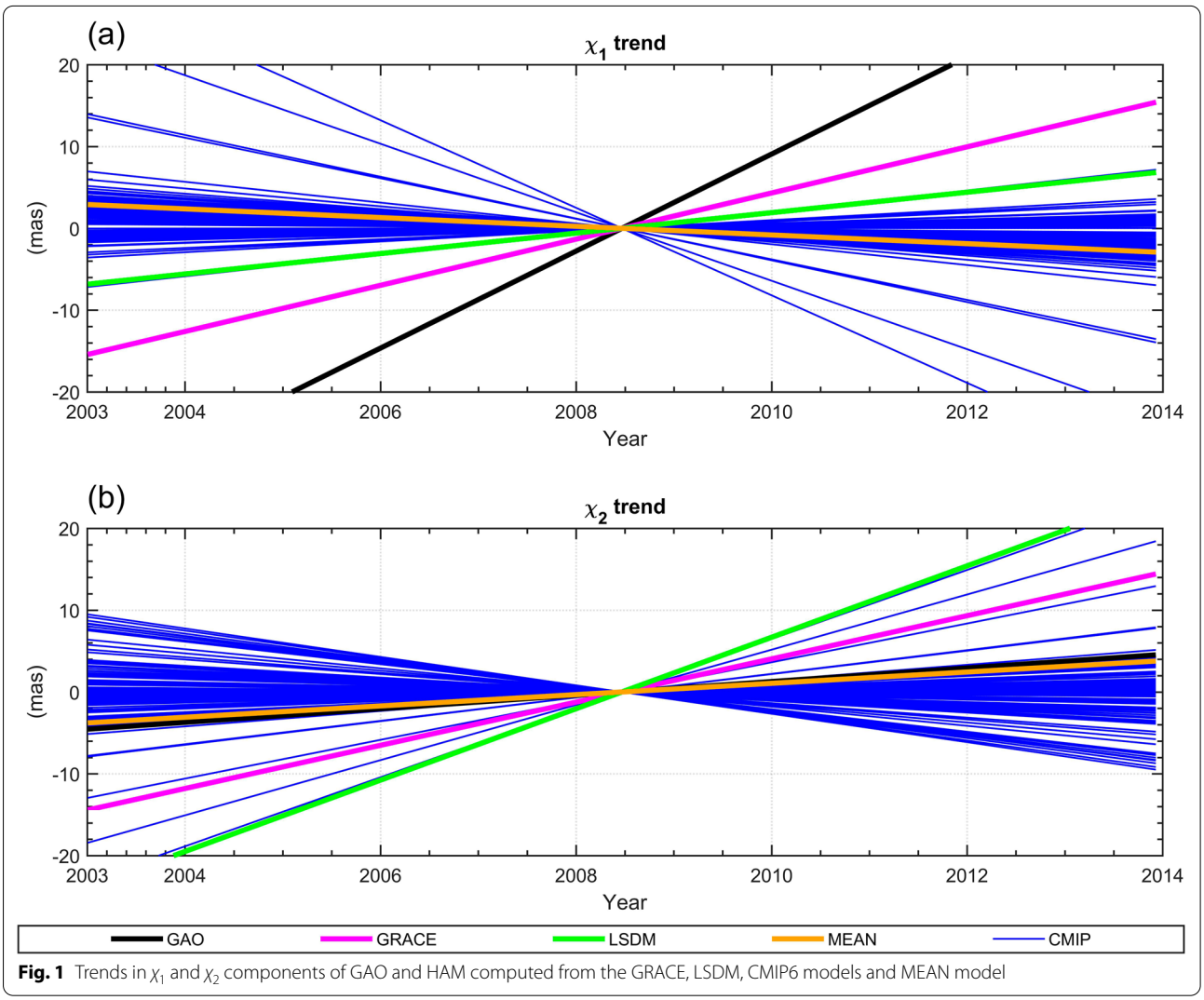

Fig. 1 Trends in χ_1 and χ_2 components of GAO and HAM computed from the GRACE, LSDM, CMIP6 models and MEAN model

Results and discussion

The results are divided into study of trends ("Trends" section), seasonal oscillations ("Seasonal variations" section), and non-seasonal oscillations ("Non-seasonal variations" section). Each section contains the analysis of HAM series determined from all the considered CMIP6 models, their comparison with GAO, and the selection of the CMIP6 model that produces the highest compatibility between HAM and GAO according to the assumed criterion. All analyses are supplemented with a study of HAM series determined from GRACE and the LSDM. In addition, we consider MEAN model, which is an average of all 99 CMIP6 models considered in this study.

Trends

The trends in HAM and GAO are shown in Fig. 1. The spread of trends is higher for the χ_1 component than for χ_2. In the case of χ_1, both GRACE-based and LSDM-based HAM agree with GAO in terms of trend sign (positive), but they both visibly underestimate the magnitude of the GAO trend. The trends of CMIP6-based HAM are positive or negative, depending on the model, and most of them are weak. There are only three climate models that provide a similar trend magnitude to that of GAO, but they all show the opposite sign. This underestimation of the GAO trend rates by CMIP6 models might occur because the models do not provide information on ice mass changes, which contribute especially to variations in the χ_1 component. This might also occur because signals from post-glacial rebound, which particularly affect trends in PM, are maintained in GAO but are not present in GRACE Level-3 data and CMIP6 models (Śliwińska et al. 2020b, 2021a). For the χ_2 component, the trend consistency between GAO and the GRACE-based or

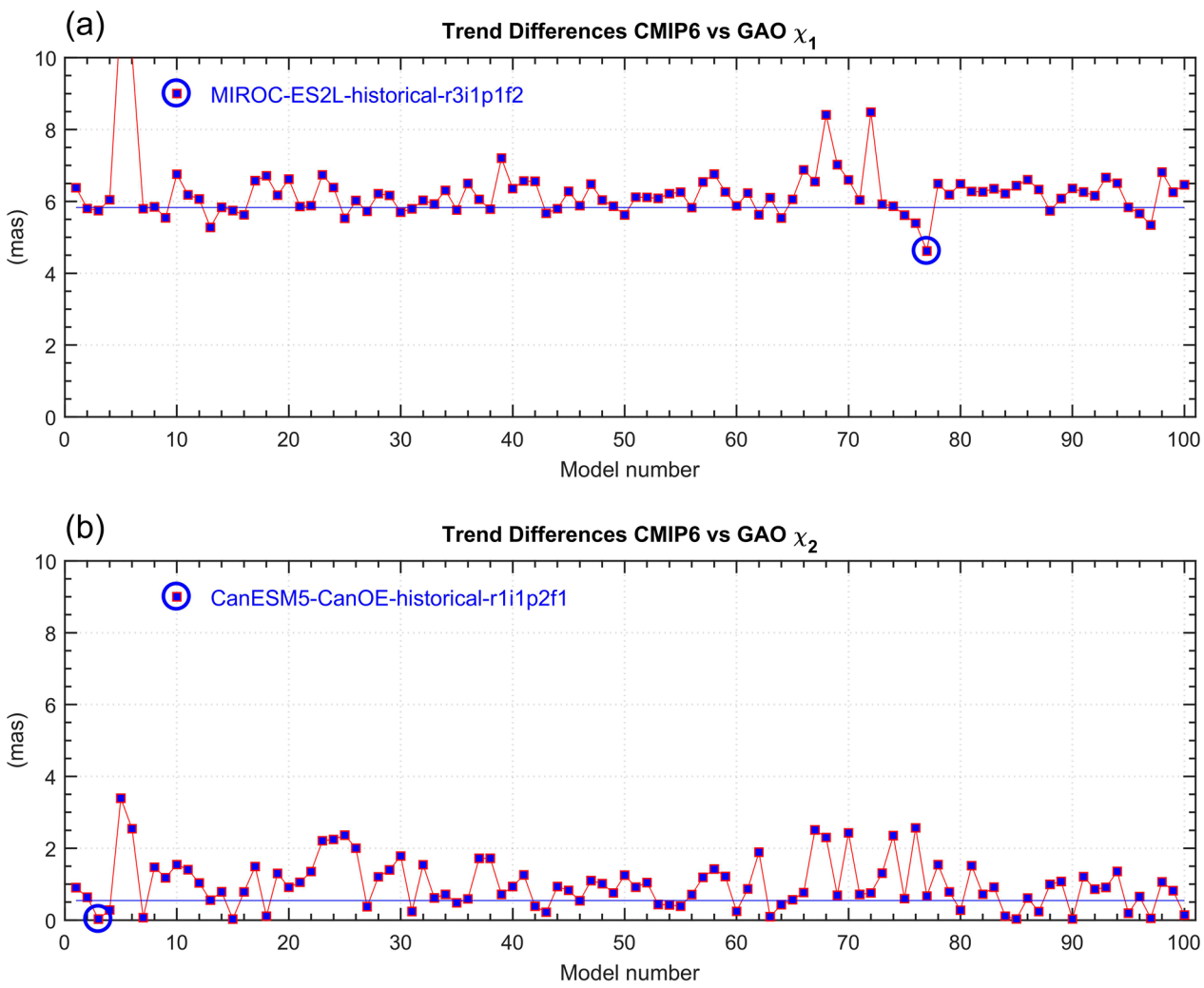

Fig. 2 Absolute values of the trend differences between GAO and HAM computed from CMIP6 in **a** χ_1 and **b** χ_2 components. Blue lines represent the first quantile. The model for which the trend differences are the smallest is indicated with a circle and description

LSDM-based HAM is higher than that for χ_1, which is consistent with results obtained in our previous research (Nastula et al. 2019; Śliwińska et al. 2020a, b, 2021a, b). There are also several CMIP6 models that provide trends that are relatively consistent with those of GAO; however, there are clear differences in trends between HAM obtained from the various CMIP6 models. It is noticeable that trend for the MEAN model is quite consistent with trend of GAO in terms of χ_2 component, however, for the case of χ_1 component this consistency is rather poor.

In order to select the optimal CMIP6 model to study HAM trends, we calculated the trend differences of GAO and each CMIP6-based HAM for each of the χ_1 and χ_2 components. We then identified the minimum value of the absolute difference between trends, which is shown in Fig. 2. The model numbers given on the x axis correspond to the numbers listed in Table 9 in Appendix (the last number, 100, corresponds to the MEAN model). Table 1 gives the differences obtained for GRACE, LSDM, MEAN model and the five CMIP6 models with the minimum values for the absolute difference between trends, given separately for χ_1 and χ_2. It is clear that the trend differences between CMIP6-based HAM and GAO are higher for χ_1 than for χ_2 and range between about 4.5 and 9.0 mas/year (except one model with difference much higher than 10.0 mas/year) (Fig. 2). Of all considered climate simulations, for the χ_1 trend, MIROC-ES2L_historical_r3i1p1f2 provided the lowest difference (4.62 mas/year). This result is similar to that obtained for LSDM-based HAM and less satisfactory than for the case of GRACE-based HAM. For the χ_2 component, the trend discrepancies were below 3.0 mas/year for almost all CMIP6 models. Four models can ensure a very high trend compliance with GAO (CanESM5-CanOE_historical_r1i1p2f1, CanESM5_historical_r1i1p2f1, MPI-ESM1-2-LR_historical_r3i1p1f1, MPI-ESM1-2-LR_historical_r8i1p1f1), with differences at the level of 0.03 mas/year. This is much better than the consistency obtained for GRACE data and the LSDM model (Table 1). However, among these four best models, there is no single model that provides the highest trend consistency with GAO for χ_1. It is also noticeable that the MEAN model provides worse trend consistency with GAO than the selected best CMIP6 models, GRACE and LSDM, which is especially apparent in χ_1. Nevertheless, in the case of χ_2 the use of the average of all CMIP6 simulations resulted in more satisfactory trend agreement with GAO than exploiting GRACE data and LSDM. For better visibility, the trends for the two chosen models, one for χ_1 and one for χ_2, are plotted in Fig. 3 (note that for χ_2 only one model is shown on the plot, but there are four models that provide the same result).

Seasonal variations

The seasonal variations in GAO and the various HAM series are shown in Fig. 4. For the χ_1 component, HAM from either GRACE, LSDM or MEAN model underestimate the amplitudes of seasonal oscillation in GAO. This supports the findings of our previous research focusing on HAM determined from these datasets (Nastula and Śliwińska 2020; Śliwińska et al. 2020a). The GRACE-, LSDM- and MEAN-based HAM series are also slightly shifted in phase with respect to the GAO (Fig. 4). Among all CMIP6-based HAM series, there are several that provide a good amplitude and phase consistency with GAO. For the χ_2 component, both GRACE and LSDM data obtain high phase agreement with GAO, but the amplitudes of the LSDM-based HAM were most consistent with those of GAO. The MEAN model provides visibly smaller amplitudes of seasonal oscillation than GRACE and LSDM. A visual inspection of the seasonal χ_2 series

Table 1 Absolute values of trend differences in χ_1 and χ_2 between GAO and HAM from CMIP6 (only the five models with smallest differences are shown)

X_1		X_2	
Model	**Difference (mas/year)**	**Model**	**Difference (mas/year)**
MIROC-ES2L_historical_r3i1p1f2	4.62	CanESM5-CanOE_historical_r1i1p2f1	0.03
GISS-E2-1-G_historical_r10i1p3f1	5.27	CanESM5_historical_r1i1p2f1	0.03
MRI-ESM2-0_historical_r4i1p1f1	5.34	MPI-ESM1-2-LR_historical_r3i1p1f1	0.03
MIROC-ES2L_historical_r2i1p1f2	5.39	MPI-ESM1-2-LR_historical_r8i1p1f1	0.03
GISS-E2-1-G_historical_r4i1p1f2	5.53	MRI-ESM2-0_historical_r4i1p1f1	0.05
GRACE	3.11	GRACE	1.81
LSDM	4.68	LSDM	3.53
MEAN	6.46	MEAN	0.14

The results obtained from GRACE, LSDM, and MEAN model are also shown

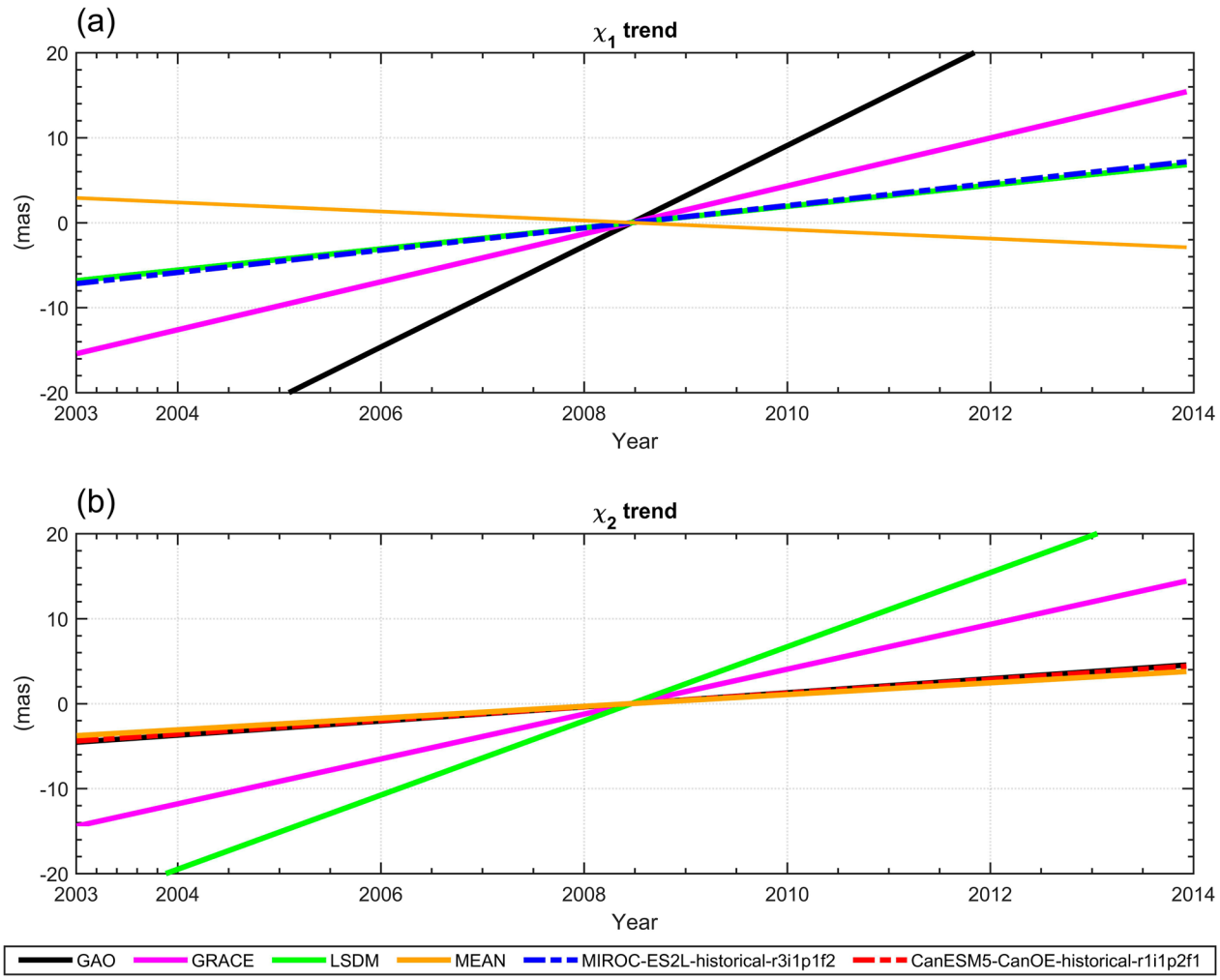

Fig. 3 The CMIP6 models best suited to GAO in terms of the trends (blue line for χ_1 in **a** and red line for χ_2 in **b**). The results obtained from GRACE, LSDM and MEAN model are also shown

shows that HAM obtained from CMIP6 models can be divided into three distinct groups: those with quite high amplitude and good phase consistency with GAO (only one model), those with quite high phase agreement with GAO but with lower amplitudes than GAO, and those with low amplitude and poor phase consistency with GAO (Fig. 4).

In order to look closer into the seasonal oscillations, we decompose these series into prograde and retrograde circular terms separately for annual and semiannual variation. Such oscillations are usually presented using phasor diagrams showing amplitudes and phases of oscillation (Fig. 5), while considering PM excitation (Brzeziński et al. 2009; Dobslaw et al. 2010; Seoane et al. 2011; Wińska et al. 2016). The diagram shows that annual oscillations play a dominant role in the seasonal spectral band, which is indicated by larger amplitudes than in the case of semiannual changes (Fig. 5). There is a wide spread of CMIP6 results in terms of phases as the vectors have different directions, especially for the annual retrograde term. Only a few CMIP6 simulations provide a high phase consistency between HAM and GAO in each considered seasonal oscillation. The GRACE- and LSDM-based HAM are characterized by satisfactory phase consistency with GAO for annual retrograde and semiannual prograde variation. The phasor diagrams also show that the CMIP6 results had a great range of amplitudes because of the variable vector length. For annual oscillations, it was possible to identify several models that provide HAM amplitudes that are similar to those of GAO, but for the semiannual term, all CMIP6-based HAM series underestimate

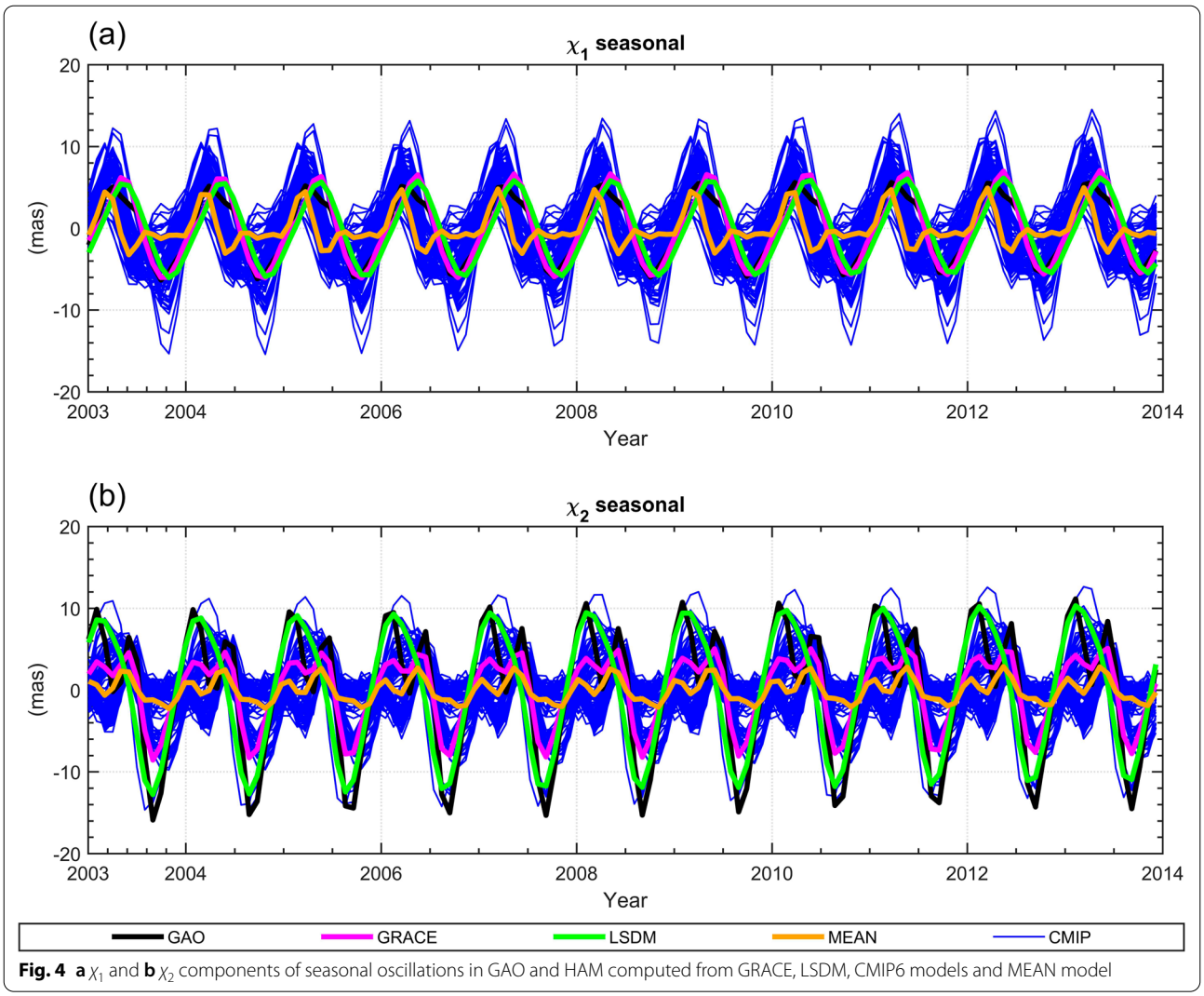

Fig. 4 **a** χ_1 and **b** χ_2 components of seasonal oscillations in GAO and HAM computed from GRACE, LSDM, CMIP6 models and MEAN model

the GAO amplitudes. Nevertheless, GRACE and LSDM data also do not allow full amplitude compliance with GAO for semiannual changes. It can be seen that only in the case of annual prograde oscillation the use of MEAN model ensures high phase consistency between HAM and GAO. For annual retrograde term, a large variation of CMIP6-based HAM amplitudes and phases results in a very small amplitude obtained from the MEAN model. This proves that averaging the results of such a large group of models does not always lead to satisfactory conclusions.

To select the most appropriate model for HAM determination in the seasonal spectral band, we sought a CMIP6 model that provides the smallest difference in either amplitude or phase of the annual and semiannual vector compared with the GAO vector. We calculated the differences in amplitude between GAO and each CMIP6-based HAM for annual prograde, annual retrograde, semiannual prograde, and semiannual retrograde terms separately. We then searched for the minimum value of the absolute difference between amplitudes. A similar procedure was then used for the phase differences.

Figure 6 shows the absolute values of differences in amplitudes and phases of annual oscillation. The discrepancies between CMIP6-based HAM and GAO amplitudes are smaller for the prograde than for the retrograde term. The differences range from about 0.1 mas to 4.5 mas for prograde oscillation, and from 1.5 mas to 6 mas for the retrograde term. Analysis of phase differences reveals that for prograde oscillation values usually do not exceed 70°. The results for the annual retrograde term are less uniform. A group of models provide a high phase consistency between HAM and GAO (with differences below 30°), while remaining HAM series are characterized by rather low phase agreement with GAO (differences above 60°). There are hardly any time series

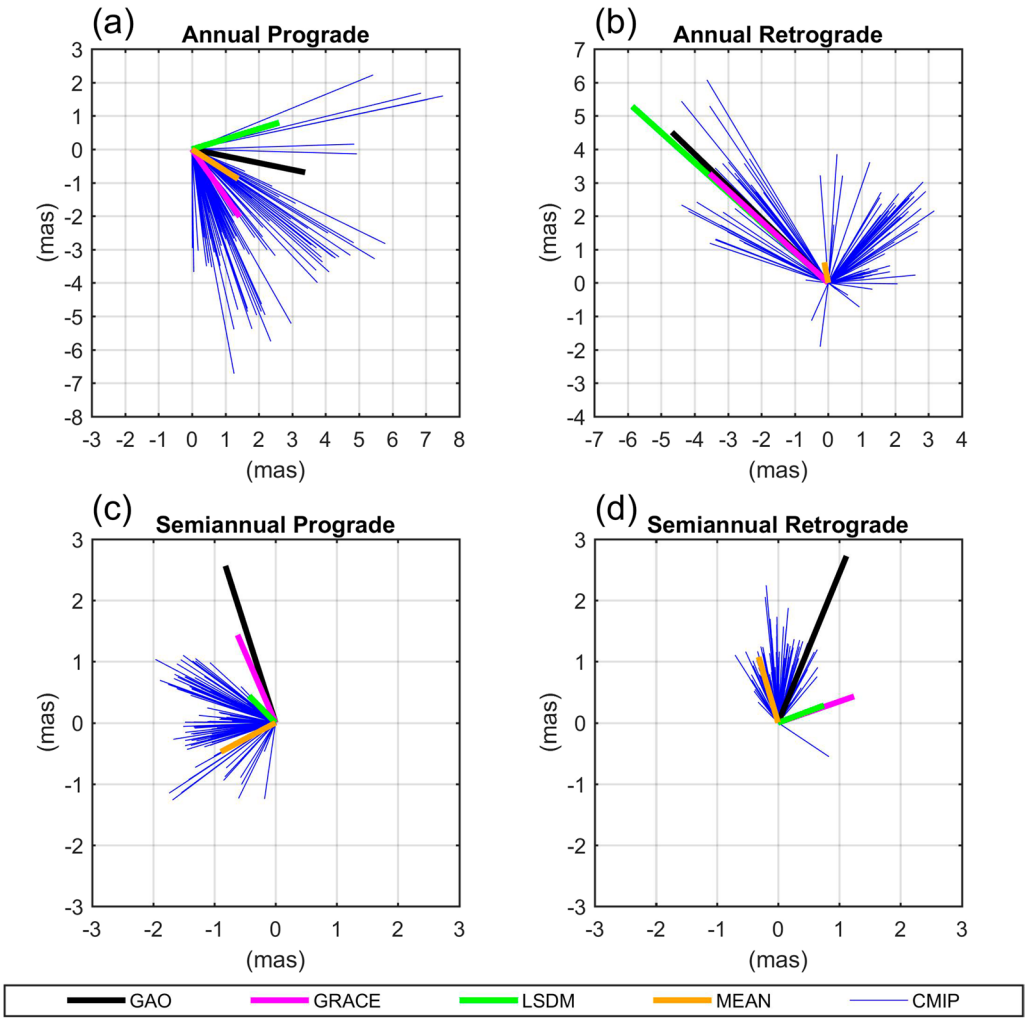

Fig. 5 Phasor diagrams of **a** annual prograde, **b** annual retrograde, **c** semiannual prograde, and **d** semiannual retrograde oscillation in GAO and HAM computed from GRACE, LSDM, CMIP6 models and MEAN model

that provide differences between 30° and 60° for annual retrograde oscillation.

Table 2 presents absolute values of amplitude differences obtained for GRACE, LSDM, MEAN model and the five best CMIP6 models (based on smallest amplitude differences), given separately for annual prograde and annual retrograde terms, while Table 3 contains the information for phase discrepancies. Based on these tables, it is possible to select a CMIP6 model that provides almost zero differences in the amplitudes and phases of the annual oscillation. However, a different model proved to be the best for prograde or retrograde amplitudes or phases: GISS-E2-1-G_historical_r10i1p1f1 for annual prograde amplitudes, GFDL-CM4_historical_r1i1p1f1 for annual retrograde amplitudes, BCC-ESM1_historical_r3i1p1f1 for the annual prograde phase, and MIROC-ES2L_historical_r2i1p1f2 for the annual retrograde phase. It is promising, however, that more than one model can be identified for the annual prograde and retrograde terms that provides higher consistency with GAO than GRACE- and LSDM-based HAM (except phase of annual retrograde oscillation, for which only one CMIP6-based HAM has smaller differences than GRACE-based HAM). Notably, results from MEAN model are generally less satisfactory than those obtained for selected CMIP6, GRACE and LSDM (except phase of annual prograde term, for which MEAN provides higher consistency with GAO than both GRACE and LSDM, which is also visible in Fig. 5).

The absolute values of differences in amplitudes and phases of semiannual oscillation are presented in Fig. 7. The discrepancies in amplitudes between CMIP6-based

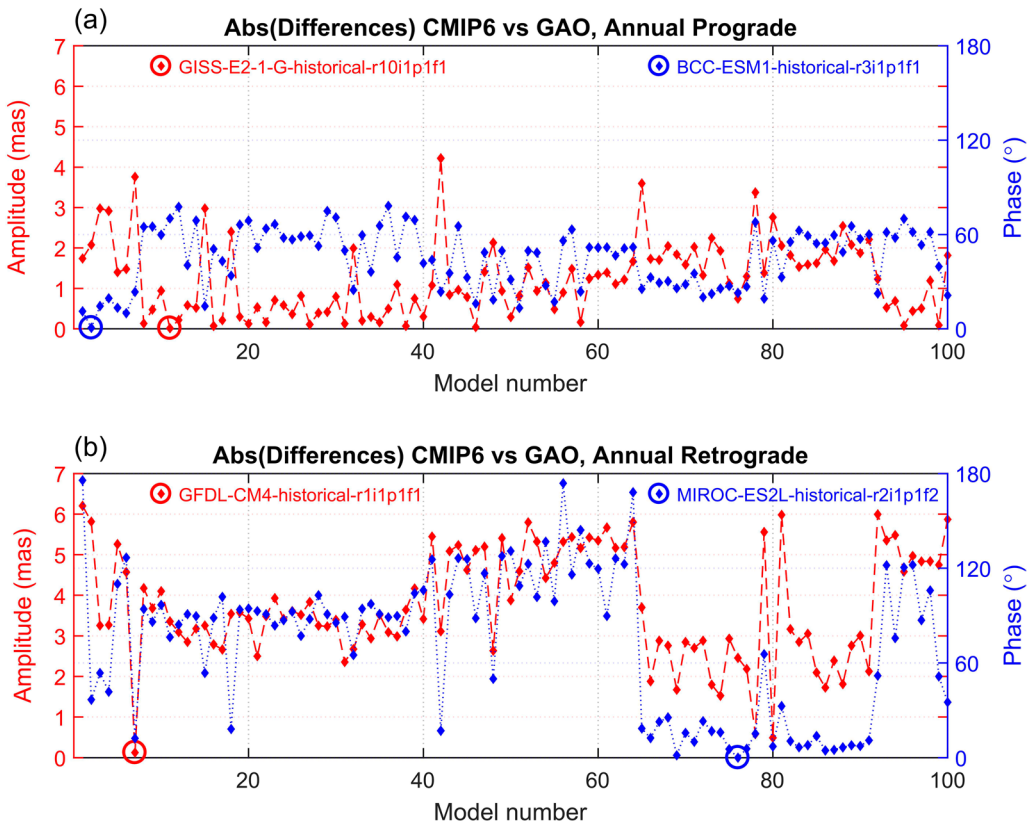

Fig. 6 Absolute values of differences in amplitudes and phases between CMIP6-based HAM and GAO for **a** annual prograde oscillation and **b** annual retrograde oscillation. The models for which the amplitude and phase differences are the smallest are indicated by circles and labels

Table 2 Absolute values of differences in amplitude of annual prograde and annual retrograde oscillation between GAO and HAM from CMIP6 (only the five models with the smallest differences are shown)

Annual prograde amplitude		Annual retrograde amplitude	
Model	**Difference (mas)**	**Model**	**Difference (mas)**
GISS-E2-1-G_historical_r10i1p1f1	0.02	GFDL-CM4_historical_r1i1p1f1	0.13
GISS-E2-1-H_historical_r1i1p5f1	0.04	MPI-ESM-1–2-HAM_historical_r2i1p1f1	0.49
GISS-E2-1-G_historical_r9i1p1f1	0.07	MPI-ESM-1–2-HAM_historical_r1i1p1f1	0.58
GISS-E2-1-G_historical_r1i1p1f2	0.07	MIROC6_historical_r9i1p1f1	1.53
MRI-ESM2-0_historical_r2i1p1f1	0.08	MIROC6_historical_r4i1p1f1	1.67
GRACE	0.98	GRACE	1.66
LSDM	0.73	LSDM	1.40
MEAN	1.82	MEAN	5.87

The results obtained from GRACE, LSDM, and MEAN model are also shown

HAM and GAO are slightly smaller for the prograde than retrograde term, which was also apparent for annual variation. The differences range from about 0.5 mas to 2.5 mas for prograde oscillation, while most of the values are between 1.0 mas and 3.0 mas for the retrograde term. Figure 7 shows that in terms of phases of semiannual oscillation, the consistency between CMIP6-based HAM and GAO is visibly higher for retrograde variation (differences below 100°) than for prograde variation (differences between 25° and 180°).

Table 3 Absolute values of differences in phase of annual prograde and annual retrograde oscillation between GAO and HAM from CMIP6 (only the five models with the smallest differences are shown)

Annual prograde phase		Annual retrograde phase	
Model	**Difference (°)**	**Model**	**Difference (°)**
BCC-ESM1_historical_r3i1p1f1	0.66	MIROC-ES2L_historical_r2i1p1f2	0.00
ACCESS-CM2_historical_r2i1p1f1	9.96	MIROC6_historical_r4i1p1f1	1.49
BCC-ESM1_historical_r2i1p1f1	11.14	MPI-ESM1-2-LR_historical_r4i1p1f1	4.56
GISS-E2-1-H_historical_r2i1p5f1	13.24	MPI-ESM1-2-LR_historical_r5i1p1f1	4.98
ACCESS-CM2_historical_r1i1p1f1	13.37	MIROC-ES2L_historical_r1i1p1f2	5.39
GRACE	43.20	GRACE	1.31
LSDM	28.51	LSDM	1.94
MEAN	21.28	MEAN	35.14

The results obtained from GRACE, LSDM, and MEAN model are also shown

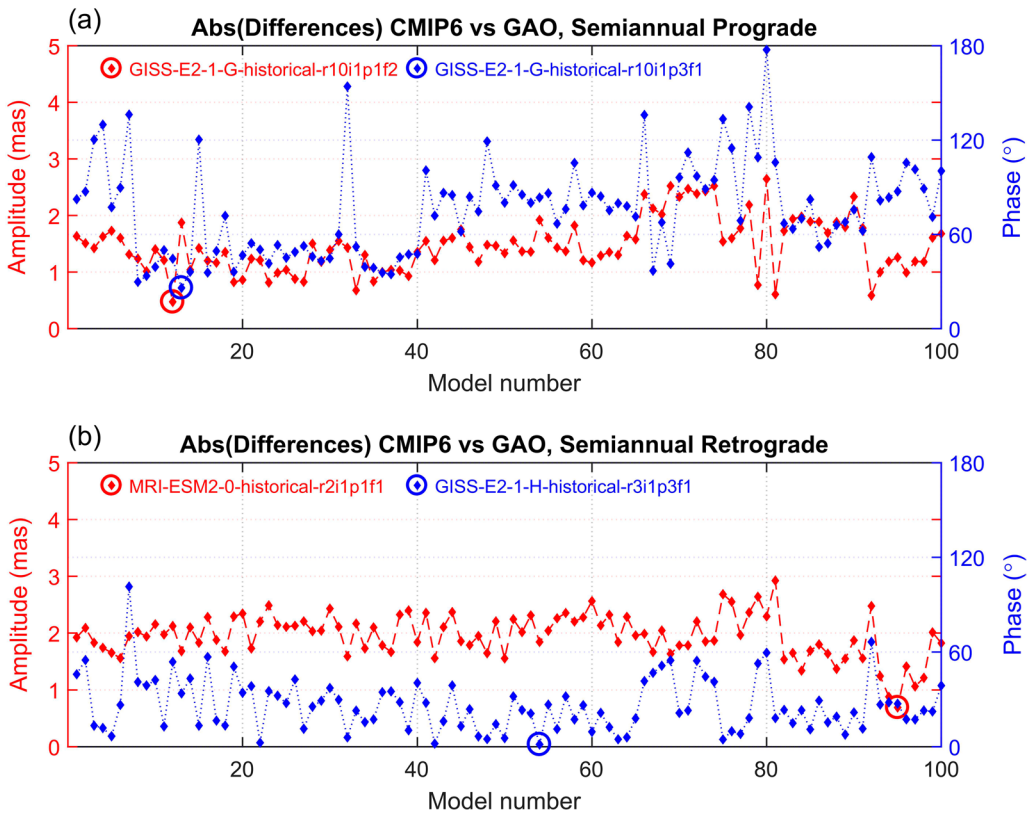

Fig. 7 Absolute values of differences in amplitudes and phases between CMIP6-based HAM and GAO for **a** semiannual prograde oscillation and **b** semiannual retrograde oscillation. The models for which the amplitude and phase differences are the smallest are indicated by circles and labels

The absolute values of differences for GRACE, LSDM, MEAN model and the five best CMIP6 models are given for amplitudes and phases of semiannual variation in Tables 4 and 5, respectively. It is possible to identify a CMIP6 model that provides amplitude differences between HAM and GAO of less than 1 mas (GISS-E2-1-G_historical_r10i1p1f2 for prograde term and MRI-ESM2-0_historical_r2i1p1f1 for retrograde term), which is definitely a more satisfactory result than for the case of HAM determined using GRACE and LSDM (Table 4).

Table 4 Absolute values of differences in amplitude of semiannual prograde and semiannual retrograde oscillation between GAO and HAM from CMIP6 (only the five models with the smallest differences are shown)

Semiannual prograde amplitude		Semiannual retrograde amplitude	
Model	**Difference (mas)**	**Model**	**Difference (mas)**
GISS-E2-1-G_historical_r10i1p1f2	0.47	MRI-ESM2-0_historical_r2i1p1f1	0.69
BCC-CSM2-MR_historical_r3i1p1f1	0.59	MRI-ESM2-0_historical_r1i2p1f1	0.88
BCC-CSM2-MR_historical_r2i1p1f1	0.61	MRI-ESM2-0_historical_r4i1p1f1	1.06
GISS-E2-1-G_historical_r7i1p1f2	0.68	MRI-ESM2-0_historical_r5i1p1f1	1.21
BCC-CSM2-MR_historical_r1i1p1f1	0.77	MRI-ESM2-0_historical_r1i1p1f1	1.24
GRACE	1.13	GRACE	1.63
LSDM	2.08	LSDM	2.15
MEAN	1.68	MEAN	1.82

The results obtained from GRACE, LSDM, and MEAN model are also shown

Table 5 Absolute values of differences in phase of semiannual prograde and semiannual retrograde oscillation between GAO and HAM from CMIP6 (only the five models with the smallest differences are shown)

Semiannual prograde phase		Semiannual retrograde phase	
Model	**Difference (°)**	**Model**	**Difference (°)**
GISS-E2-1-G_historical_r10i1p3f1	25.96	GISS-E2-1-H_historical_r3i1p3f1	1.42
GISS-E2-1-G-CC_historical_r1i1p1f1	29.78	ACCESS-ESM1-5_historical_r2i1p1f1	1.93
GISS-E2-1-G_historical_r101i1p1f1	33.56	GISS-E2-1-G_historical_r3i1p1f1	2.50
GISS-E2-1-G_historical_r8i1p3f1	34.67	MIROC-ES2L_historical_r1i1p1f2	4.64
GISS-E2-1-G_historical_r8i1p1f2	35.62	GISS-E2-1-H_historical_r8i1p1f1	4.68
GRACE	5.68	GRACE	48.58
LSDM	26.84	LSDM	47.06
MEAN	100.32	MEAN	38.73

The results obtained from GRACE, LSDM, and MEAN model are also shown

A similar situation occurs for the retrograde phases, for which the GISS-E2-1-H_historical_r3i1p3f1 model provides an almost perfect fit to the GAO vector (difference below 2°), while the use of either GRACE or LSDM results in differences of nearly 50°. Only the phases of semiannual prograde variation are better determined by GRACE (phase difference is below 6°) than by the best CMIP6 model (GISS-E2-1-G_historical_r10i1p3f1 model, phase difference as high as 26°) (Table 5). In terms of semiannual oscillation, the use of MEAN model enables to obtain higher consistency between HAM and GAO than exploiting LSDM (except for the phase of semiannual prograde term), but not as satisfactory as in the case of GRACE or selected CMIP6 models.

To further aid the selection of the best CMIP6 models for HAM determination in seasonal spectral band, the phasor diagrams are redrawn to include only the chosen CMIP6 models, GAO, GRACE, LSDM and MEAN model (Fig. 8). It is not possible to identify a single model that provides the best agreement between HAM and GAO in terms of both amplitude and phase. The chosen models are also different for prograde and retrograde terms. Noticeably, the models that provide the best phase consistency between HAM and GAO visibly underestimate the amplitudes of GAO. Nevertheless, in general, the selected models improve consistency between HAM and GAO compared with HAM series based on GRACE, LSDM or MEAN model (except the case of phase for semiannual prograde term, for which GRACE provides the best result).

Non-seasonal variations

An analysis of non-seasonal variations in HAM and GAO is presented in Fig. 9. The results for CMIP6 models are very diverse as the series are characterized by different phases (Fig. 9). Although it is difficult to identify series with a similar time course, it can be observed that, as in the case of GAO, GRACE-based HAM and LSDM-based HAM, amplitudes of non-seasonal oscillations in CMIP6-based HAM series are generally higher for χ_2

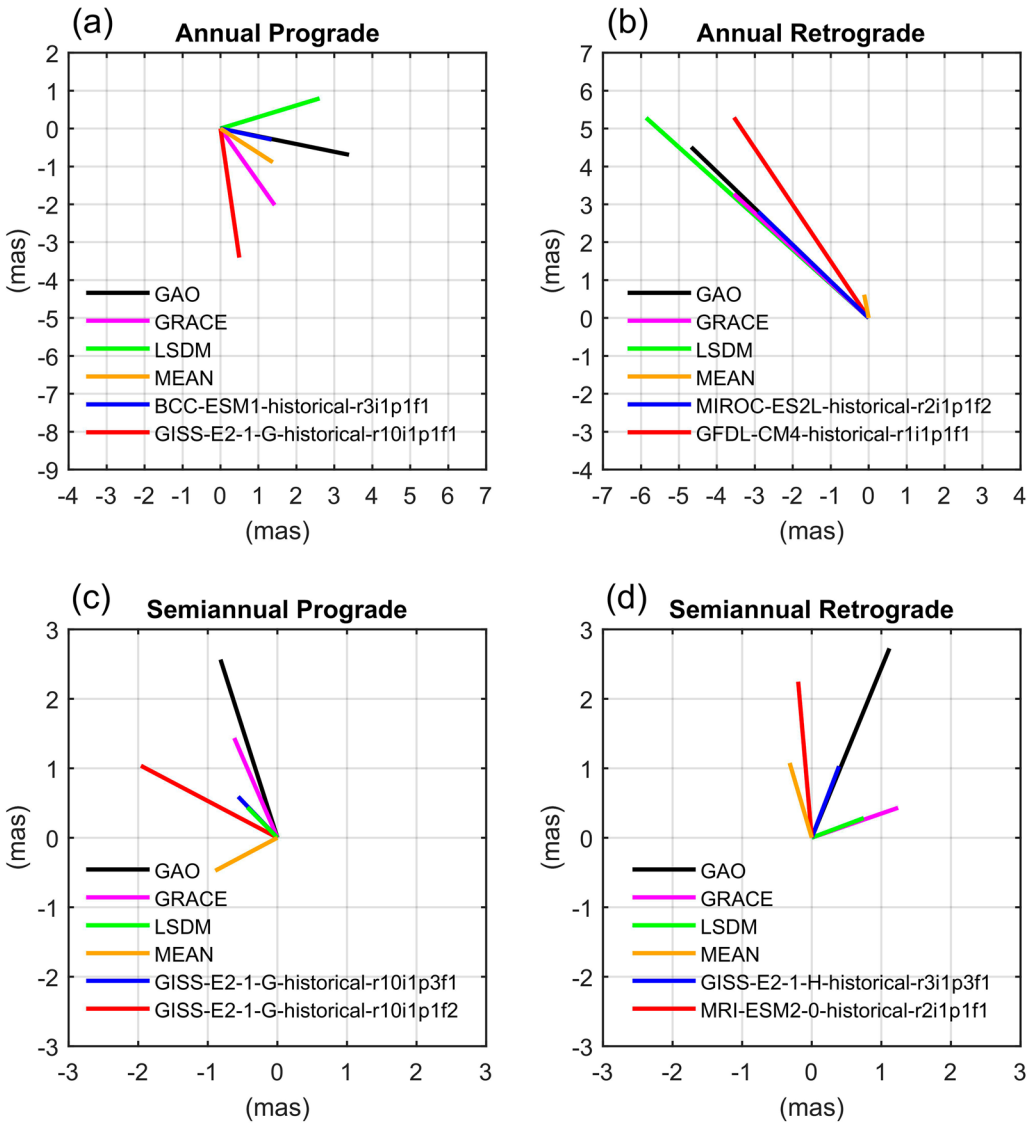

Fig. 8 Phasor diagrams of **a** annual prograde; **b** annual retrograde; **c** semiannual retrograde; and **d** semiannual retrograde oscillation in GAO and HAM computed from GRACE, LSDM, MEAN model and best fitted models selected from CMIP6 in terms of amplitude agreement (red vector) and phase agreement (blue vector)

than for χ_1. This is related to the spatial distribution of the main continents and oceans, which makes χ_2 more sensitive to mass changes over land. There is a higher consistency of GRACE- and LSDM-based HAM with GAO for the χ_2 component, which supports the results of previous research (Nastula et al. 2019; Seoane et al. 2011; Śliwińska et al. 2019, 2020a; Wińska et al. 2017). Notably, series obtained from the MEAN model do not agree well with GAO. This is especially visible in χ_2 around mid-2007, when GAO, GRACE- and LSDM-based HAM reach minimum but the HAM determined from the MEAN model exhibit maximum.

We introduced two criteria for studying the compatibility between HAM and GAO in the non-seasonal spectral band: a low difference in variance of the series and high correlation coefficients. We calculated the differences in variance of the χ_1 and χ_2 components between GAO and each CMIP6-based HAM and then searched for the minimum value of the absolute difference. We also computed correlation coefficients between GAO and

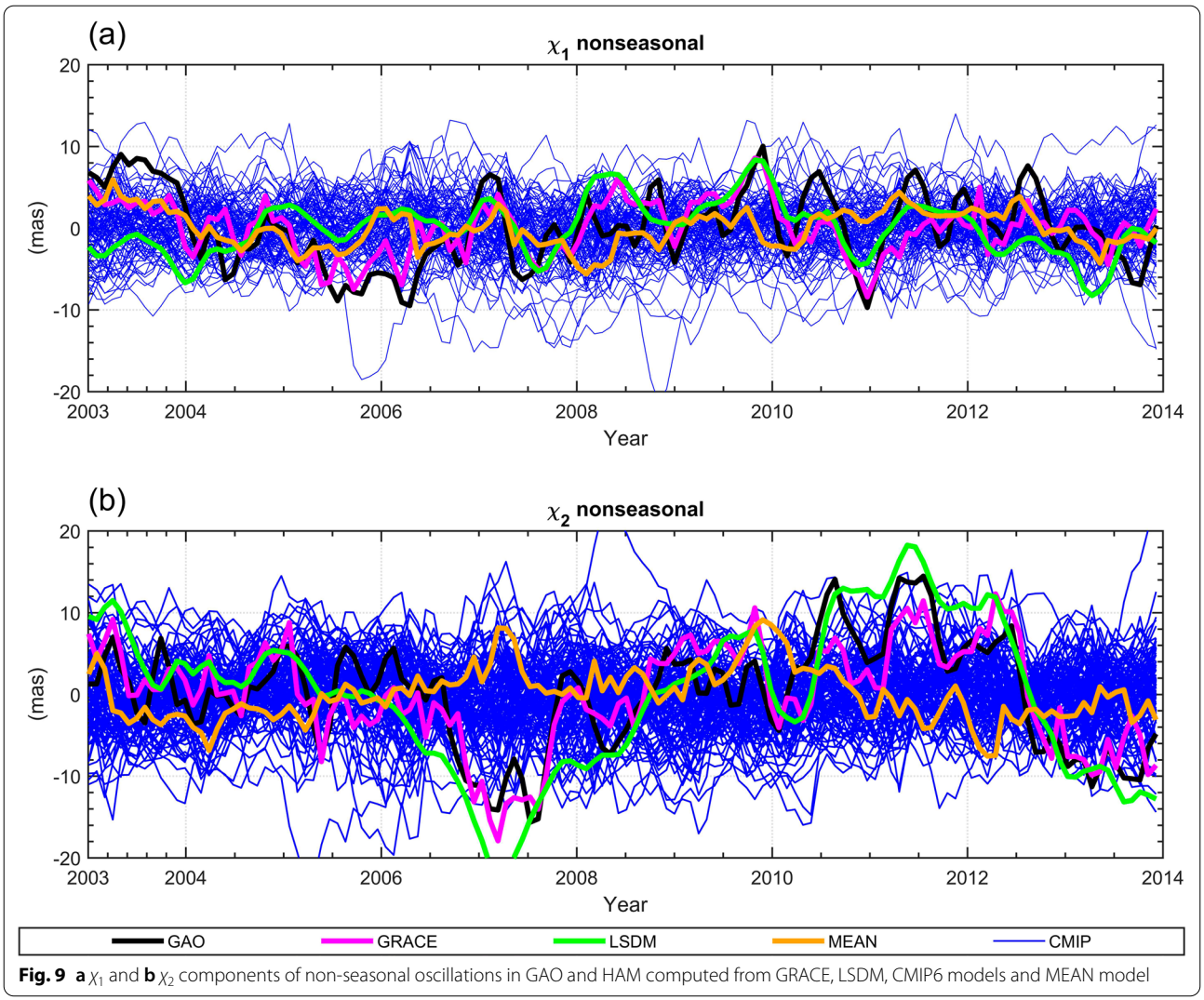

Fig. 9 **a** χ_1 and **b** χ_2 components of non-seasonal oscillations in GAO and HAM computed from GRACE, LSDM, CMIP6 models and MEAN model

each CMIP6-based HAM for the χ_1 and χ_2 components and identified the maximum value.

The absolute values of differences in variance of non-seasonal oscillation are displayed for each CMIP6 model in Fig. 10. Table 6 gives the differences obtained for GRACE, LSDM, MEAN model and the CMIP6 models for which these values were the smallest. Figure 10 shows that in the case of the χ_1 component, the variance differences in most cases did not exceed 20 mas, whereas these values could reach 40 mas for the χ_2 component (Fig. 10). The higher differences observed for the χ_2 component may result from the generally greater variance of the time series (Fig. 9). The results presented in Table 6 show that there are several CMIP6 models that provide high variance consistency between HAM and GAO. For both χ_1 and χ_2, the use of the GFDL-CM4_historical_r1i1p1f1 model produces the smallest variance differences (0.55 mas for χ_1 and 0.02 mas for χ_2). In contrast, the differences obtained for GRACE data are as high as 10.51 mas and 3.55 mas for χ_1 and χ_2, respectively, while for LSDM they reach values of 10.75 mas and 40.51 mas for χ_1 and χ_2, respectively. Notably, the differences observed for the MEAN model reaches visibly higher values than those obtained for the selected CMIP6, which indicates that also for non-seasonal spectral band averaging all climate models does not lead to a satisfactory level of consistency between HAM and GAO.

Figure 11 presents correlation coefficients between GAO and various CMIP6-based HAM, and Table 7 presents values for GRACE, LSDM, MEAN model and the five CMIP6 models for which the correlation coefficients are the highest. In general, correlations are at a similar level for both χ_1 and χ_2 and do not exceed 0.60 (Fig. 11). There are also several negative values, which indicates a phase mismatch between HAM and GAO. The correlation coefficients given in Table 7 show that in the

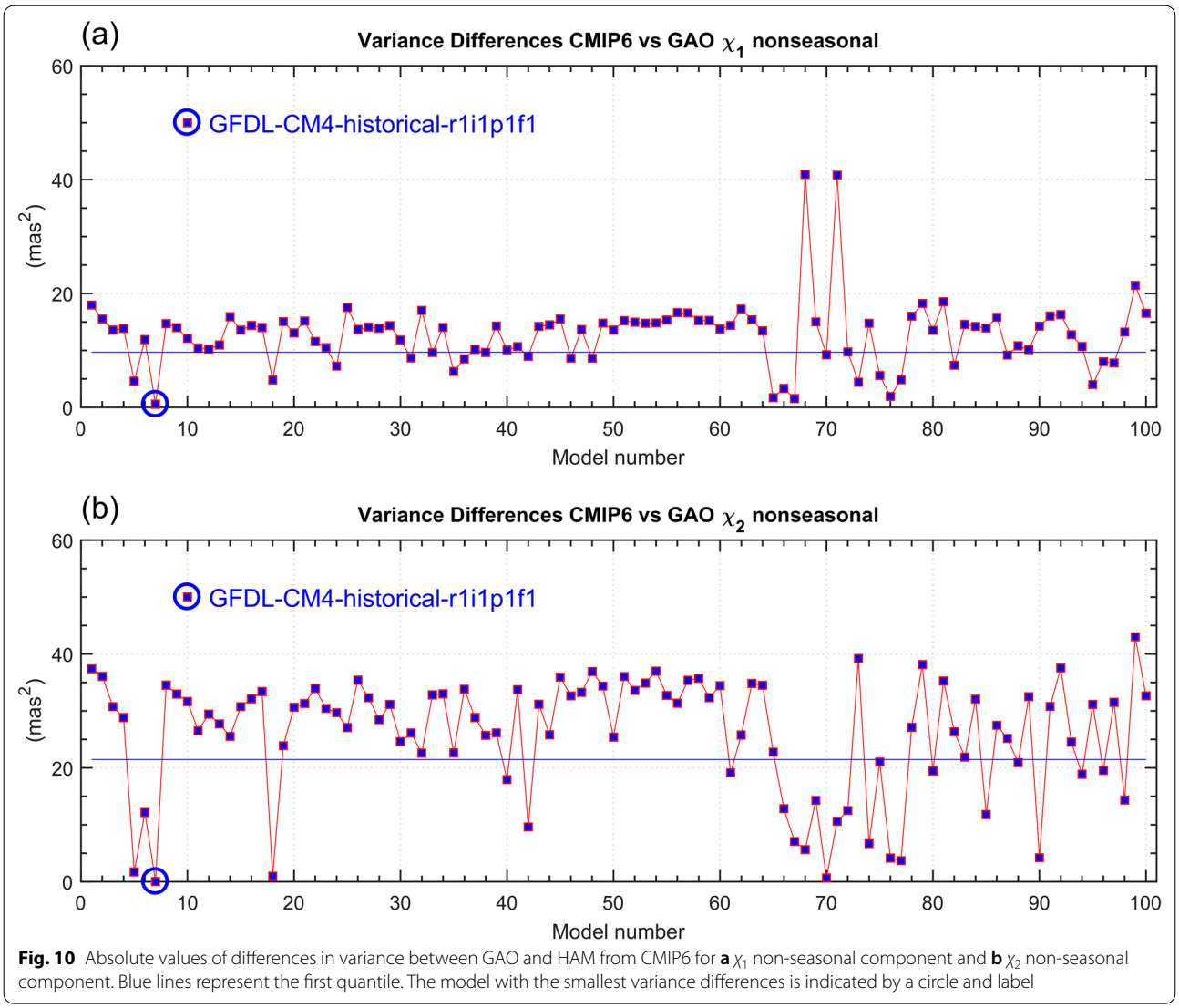

Fig. 10 Absolute values of differences in variance between GAO and HAM from CMIP6 for **a** χ_1 non-seasonal component and **b** χ_2 non-seasonal component. Blue lines represent the first quantile. The model with the smallest variance differences is indicated by a circle and label

Table 6 Absolute values of differences of non-seasonal variance in χ_1 and χ_2 between GAO and HAM from CMIP6 (only the five models with the smallest differences are shown)

X_1		X_2	
Model	**Difference (mas)**	**Model**	**Difference (mas)**
GFDL-CM4_historical_r1i1p1f1	0.55	GFDL-CM4_historical_r1i1p1f1	0.02
MIROC6_historical_r1i1p1f1	1.53	MIROC6_historical_r5i1p1f1	0.65
ACCESS-ESM1-5_historical_r3i1p1f1	1.69	ACCESS-ESM1-5_historical_r1i1p1f1	0.94
MIROC-ES2L_historical_r2i1p1f2	1.92	ACCESS-CM2_historical_r1i1p1f1	1.69
MIROC6_historical_r10i1p1f1	3.32	MIROC-ES2L_historical_r3i1p1f2	3.68
GRACE	10.51	GRACE	3.55
LSDM	10.75	LSDM	40.51
MEAN	16.51	MEAN	32.63

The results obtained from GRACE,LSDM, and MEAN model are also shown

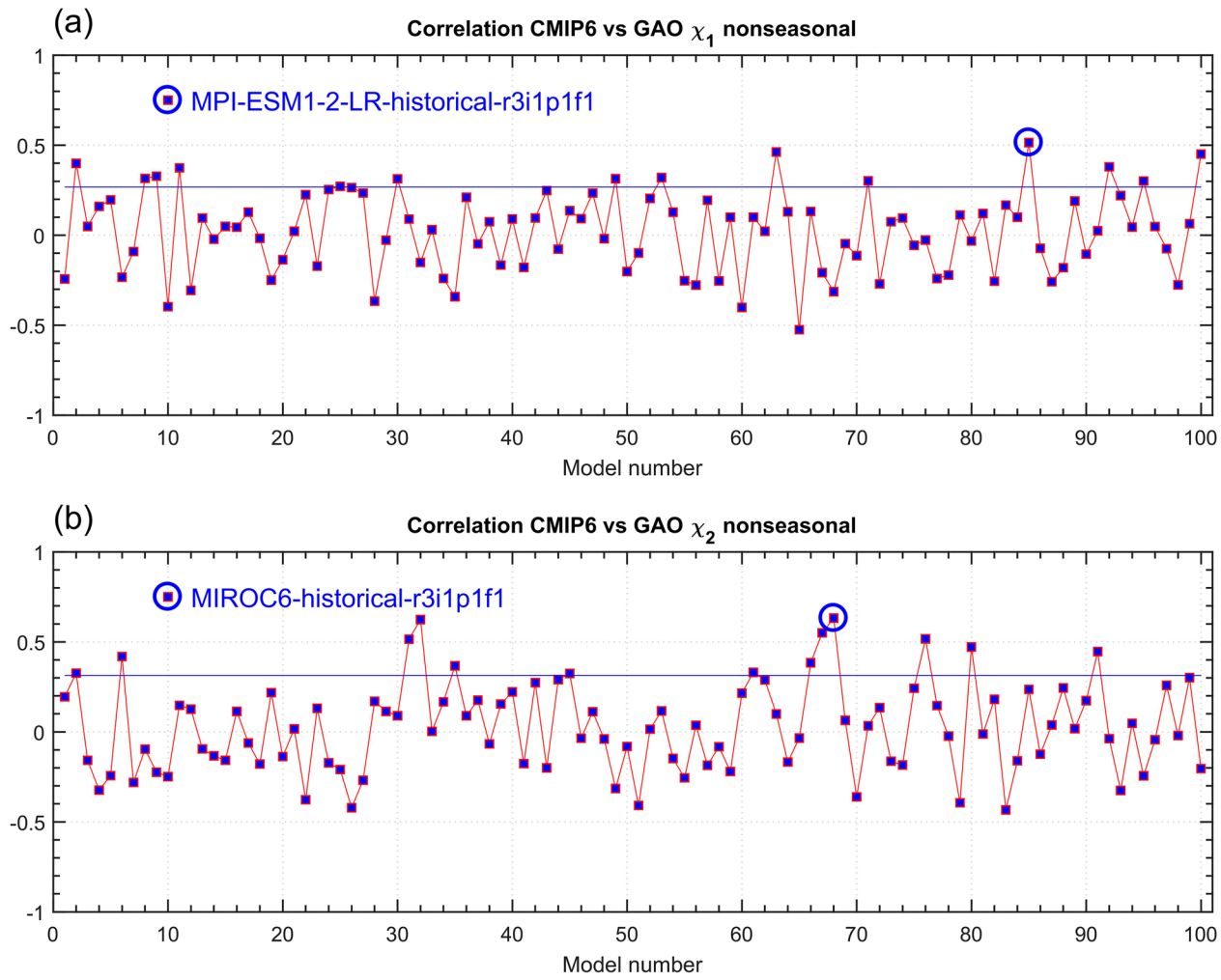

Fig. 11 Correlation coefficients between GAO and HAM from CMIP6 for **a** χ_1 non-seasonal component and **b** χ_2 non-seasonal component. Blue lines represent the first quantile. The model with the highest correlation coefficients is indicated by a circle and label

Table 7 Correlation coefficients between GAO and HAM from CMIP6 for χ_1 and χ_2 (only the five models with the highest correlation coefficients are shown)

X_1		X_2	
Model	**Correlation**	**Model**	**Correlation**
MPI-ESM1-2-LR_historical_r3i1p1f1	0.51	MIROC6_historical_r3i1p1f1	0.63
GISS-E2-1-H_historical_r8i1p1f1	0.46	CanESM5_historical_r23i1p1f1	0.62
BCC-ESM1_historical_r1i1p1f1	0.45	MIROC6_historical_r1i1p1f1	0.55
BCC-ESM1_historical_r3i1p1f1	0.40	MIROC-ES2L_historical_r2i1p1f2	0.52
BCC-CSM2-MR_historical_r3i1p1f1	0.38	GISS-E2-1-G_historical_r6i1p3f1	0.52
GRACE	0.68	GRACE	0.84
LSDM	0.28	LSDM	0.84
MEAN	0.11	MEAN	0.41

The results obtained from GRACE, LSDM, and MEAN model are also shown

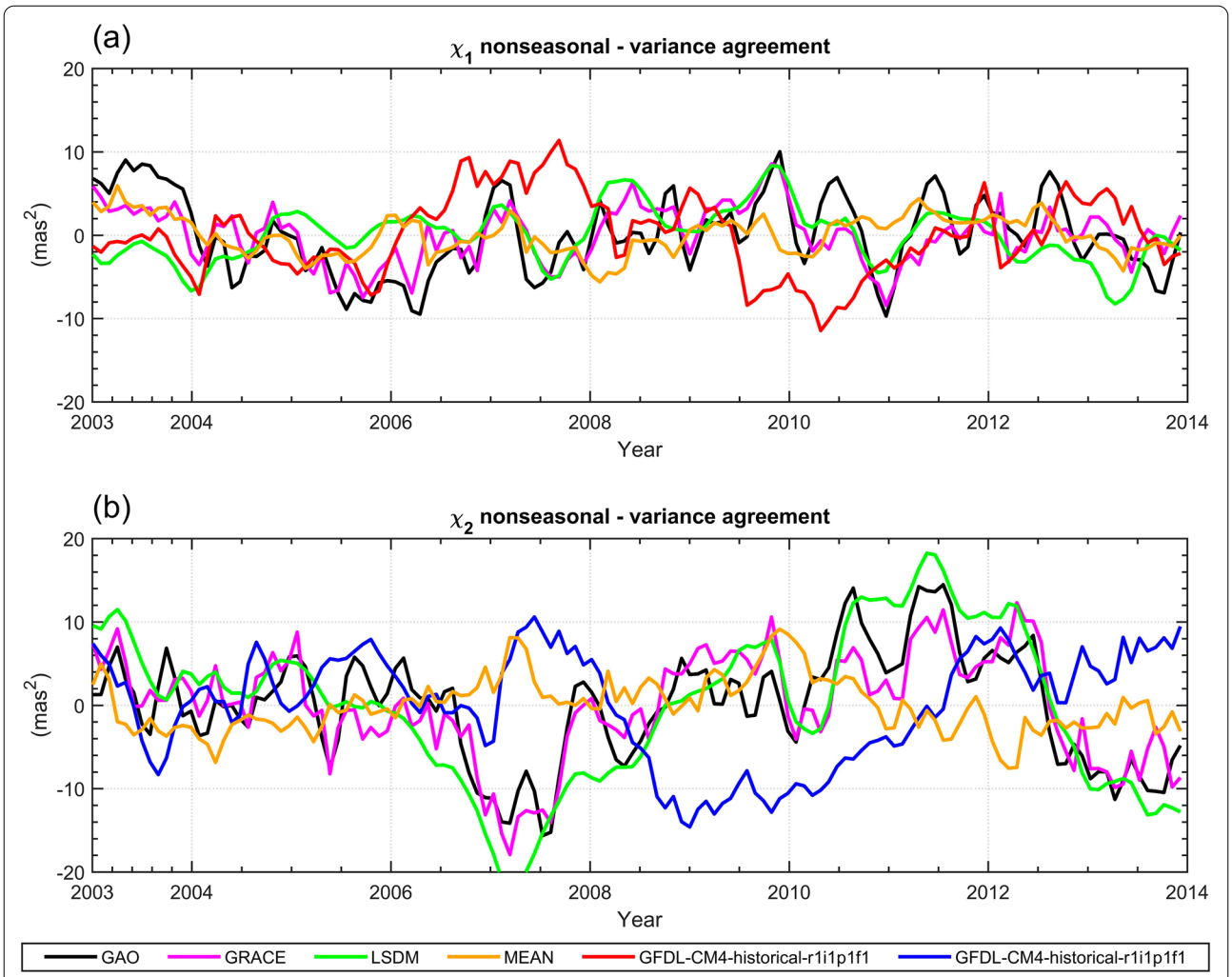

Fig. 12 The models best suited to GAO in terms of the smallest difference in variance of non-seasonal variations (red line for χ_1 in **a** and blue line for χ_2 in **b**). The results obtained from GRACE, LSDM and MEAN model are also shown

non-seasonal spectral band, none of the climate models provide as high correlations with GAO as in the case of GRACE-based HAM. However, there are several CMIP6-based HAM series that are characterized by more satisfactory correlations than HAM computed using LSDM (for χ_1 only). The CMIP6 models that were selected to ensure highest correlations between HAM and GAO are MPI-ESM1-2-LR_historical_r3i1p1f1 for χ_1 (correlation coefficient equal to 0.51) and MIROC6_historical_r3i1p1f1 for χ_2 (correlation coefficient equal to 0.63). The correlations for the MEAN model are apparently lower than values received form GRACE, LSDM and selected CMIP6.

The models chosen as best for determining non-seasonal HAM variations according to the assumed criteria are plotted in Fig. 12 (smallest variance difference) and Fig. 13 (highest correlation coefficient), and compared with GAO, GRACE-based HAM, LSDM-based HAM and HAM computed from the MEAN model. It should be noted that the series that have the best variance consistency with GAO are slightly out of phase with respect to the reference data, which is particularly noticeable in the case of the χ_2 component. The CMIP6-based HAM series that are best correlated with GAO are in reasonable amplitude agreement for the χ_2 component but they underestimate GAO amplitudes for the χ_1 component. This makes it difficult to select one CMIP6 model that

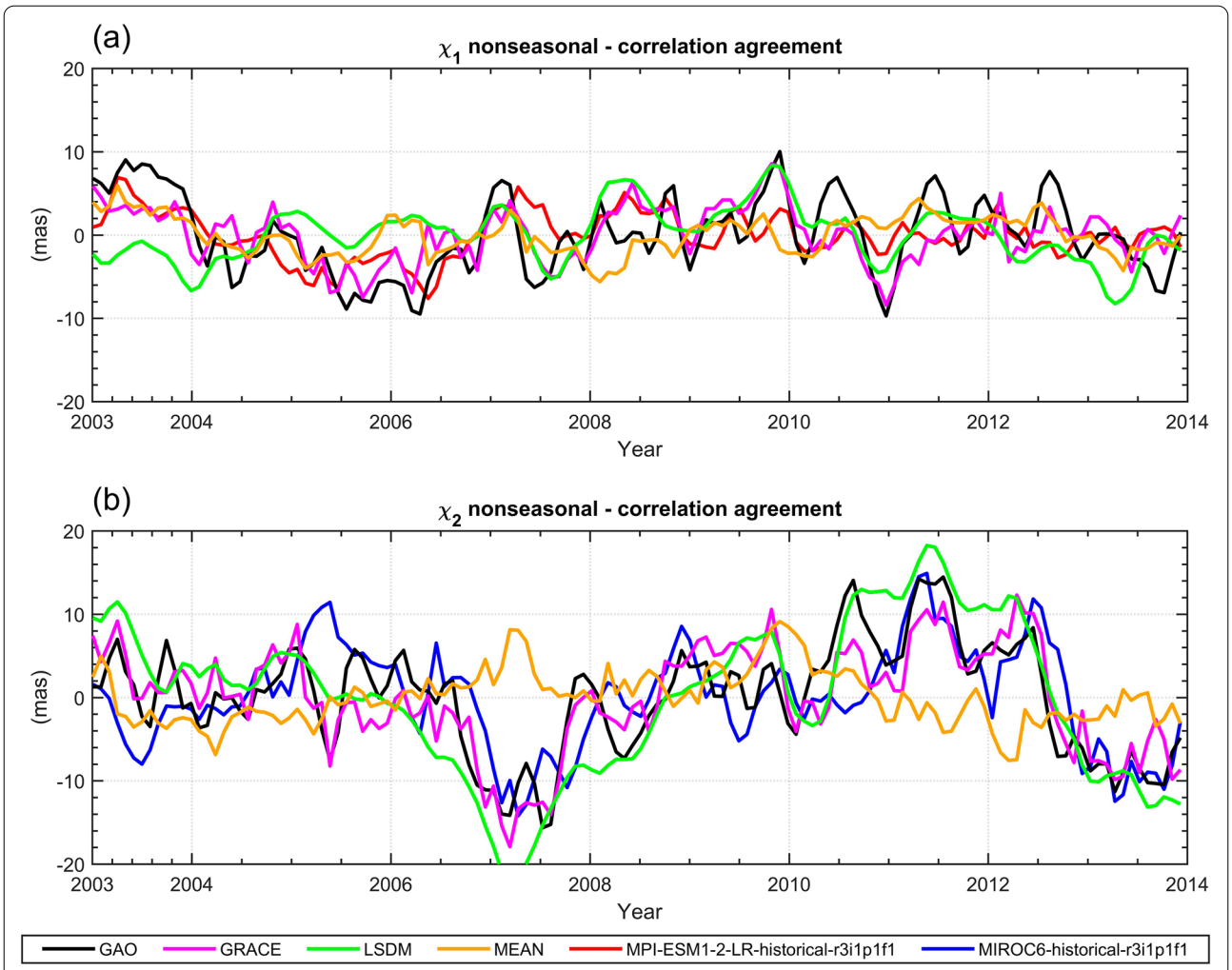

Fig. 13 The models best suited to GAO in terms of the highest correlation coefficients (red line for χ_1 in Fig. 13a and blue line for χ_2 in Fig. 13b). The results obtained from GRACE, LSDM and MEAN model are also shown

will provide the highest possible consistency with GAO in terms of both variance agreement and correlation coefficients.

Summary and conclusions

This paper presented the first preliminary analyses aimed at checking the usefulness of CMIP6 data in HAM estimation HAM determined using soil moisture and snow water variables obtained from 99 historical models made available under the CMIP6 were analysed after their decomposition into trends, seasonal oscillations, and non-seasonal oscillations. Each series was evaluated with reference to GAO and compared with HAM computed from GRACE data, the LSDM and the mean of all considered models (MEAN model).

In terms of trends, some CMIP6 models show high consistency with GAO for the χ_2 component (trend difference equal to 0.03 mas/year for the best model), but trend differences between CMIP6-based HAM and GAO in the case of χ_1 are remarkable (trend difference equal to 4.62 mas/year for the best model). This may be because climate models do not contain information about ice mass changes in the polar regions, which are likely to influence PM trends (Śliwińska et al. 2021b). For seasonal oscillations, several models provide an almost perfect fit to the GAO for amplitudes (amplitude differences for best models are equal to 0.02 mas and 0.13 mas for the prograde and retrograde term, respectively) and phases of annual oscillation (phase differences for best models are equal to 0.66° and 0 for the prograde and retrograde term, respectively). However, most of the CMIP6-based HAM series underestimate GAO amplitudes for semiannual variation. For non-seasonal oscillation, climate models were selected that provide high consistency between

HAM and GAO in terms of time series variability (the variance differences for the best models were 0.55 mas and 0.02 mas for χ_1 and χ_2, respectively) and correlation with GAO (correlation coefficients for best models are equal to 0.51 and 0.63 for χ_1 and χ_2, respectively). However, although several CMIP6-based HAM series are well correlated with GAO, they provide lower correlation coefficients than HAM determined using GRACE.

In general, identification of the most suitable climate model for HAM is a challenging task. The selection depends on several factors, such as the considered oscillation, the analysed equatorial component of HAM, and the criteria applied to the validation. It should be noted that the HAM series that are consistent with GAO in terms of amplitude usually do not exhibit high phase coherence with GAO, and vice versa. Therefore, it is essential to use another criterion for HAM evaluation that would combine both amplitude and phase compatibility tests. A good solution would be to create a single criterion that takes into account both satisfactory amplitude and phase capability. Models that do not meet assumed amplitude consistency with GAO, even though they provide high phase compliance, should be excluded from further research, and vice versa. It will also be important to choose not a single best model that meets the assumed criteria, but a group of models, which will widen the set of potential climate data that can be used in the determination of HAM.

Here, we also considered a mean of all 99 CMIP6 models. However, simply averaging the results is not a good solution as this study has shown that consistency between HAM and GAO is better for several individual models than for the MEAN model. Therefore, while determining a possible combination of CMIP6 models, it is necessary to assess the impact of each model due to e.g. poor agreement with GAO. The use of weighting of individual models would allow to obtain the highest possible compatibility between CMIP6-based HAM and GAO.

Overall, the correspondence between GAO and HAM received from CMIP6 is generally lower than the previously obtained consistency between GAO and HAM from GRACE (e.g. Śliwińska et al. 2021b). However, it may be possible to find one or a few CMIP6 models from among the almost 100 available that provides a HAM series more compatible with GAO than HAM from GRACE or LSDM, especially in annual oscillations. Nevertheless, none of the CMIP6 models provides such a high correlation between HAM and GAO in terms of non-seasonal changes as the GRACE mission data. Therefore, the gravity field models obtained from the GRACE mission observations are a more appropriate dataset for the HAM study. However, it should be kept in mind that the GRACE data also have some disadvantages, such as the length of the time series (only 15 years), which may not be sufficient for the purpose of studying PM changes induced by climate change. Although the successor of GRACE, GRACE-FO was launched in 2018, there is a data gap between the two missions of approximately one year, making it necessary to fill this gap with different observations or applying advanced interpolation procedures. Therefore, it is important to look for other data sources that can be used to study changes in PM, which are characterized by a longer period of availability than GRACE, such as the CMIP6 climate models.

The issue of using climate data to interpret PM disturbances caused by the continental hydrosphere requires further, more advanced analysis. In particular, a more detailed comparative analysis of individual CMIP6 scenarios is needed. For this purpose, the different realizations of one model provided by the same institute should be compared thoroughly. Such realizations vary in terms of initial conditions, physical properties of atmosphere, oceans, hydrosphere, and climate forcing induced by e.g. solar radiation, concentration of greenhouse gases in the atmosphere, and volcanic eruptions (Taylor et al. 2018). Improved understanding the physical causes of the differences between models is also required. In general, conclusions from our preliminary study are promising, but the research needs to be expanded especially in the field of the internal consistency between individual models. The scope of potential analyses of the use of climate data to interpret changes in the PM excitation is very wide, and this work is only an introduction to further, more focused research.

It should also be kept in mind that although we studied climate models only for the period of GRACE activity, the models can allow HAM analysis from 1850 up to 2100. This provides a unique opportunity to study the impact of climate change on variations in HAM both in the past and in the future, and such research should be carried out as the next step. Nevertheless, such a study requires long observations and predictions of pole coordinates, as well as long series of AAM and OAM to act as a reference for the quality assessment of CMIP6-based HAM. Since such data necessary for the CMIP6-based HAM assessment between 1850 and 2100 is not available for such a long period of time, CMIP6 models could be selected based on a comparison with GAO for a shorter period (for which AAM, OAM, and PM are available), and then use these models to analyse the past and future changes to the HAM for the period when no other data are available. This will be an important step in studying the effects of climate change on the movement of the pole.

Appendix

See Tables 8 and 9.

Table 8 List of the CMIP6 global climate models analysed and associated model information

Model	Grid resolution for land components	Institution and country	Reference
ACCESS-CM2	250 km	Commonwealth Scientific and Industrial Research Organisation (CSIRO), Australia	Hirst et al. (2015)
ACCESS-ESM1-5	250 km	Commonwealth Scientific and Industrial Research Organisation (CSIRO), Australia	Ziehn et al. (2019)
BCC-CSM2-MR	100 km	Beijing Climate Center (BCC), China	Wu et al. (2019)
BCC-ESM1	250 km	Beijing Climate Center (BCC), China	Wu et al. (2020)
CanESM5	500 km	Canadian Centre for Climate Modelling and Analysis, Environment and Climate Change, Canada	Swart et al. (2019)
CanESM5-CanOE	500 km	Canadian Centre for Climate Modelling and Analysis, Environment and Climate Change, Canada	Swart et al. (2019)
GFDL-CM4	100 km	National Oceanic and Atmospheric Administration's Geophysical Fluid Dynamics Laboratory (NOAA GFDL), USA	Adcroft et al. (2019)
GISS-E2-1-G	250 km	National Aeronautics and Space Administration's Goddard Institute for Space Studies (NASA GISS), USA	Goddard Institute and for Space Studies (NASA, GISS), (2019)
GISS-E2-1-G-CC	250 km	National Aeronautics and Space Administration's Goddard Institute for Space Studies (NASA GISS), USA	Goddard Institute and for Space Studies (NASA, GISS), (2019)
GISS-E2-1-H	250 km	National Aeronautics and Space Administration's Goddard Institute for Space Studies (NASA GISS), USA	Kelley et al. (2020)
MIROC6	250 km	Japan Agency for Marine-Earth Science and Technology (JAMSTEC), Atmosphere and Ocean Research Institute (AORI), National Institute for Environmental Studies (NIES), Japan	Shiogama et al. (2019)
MIROC-ES2L	500 km	Japan Agency for Marine-Earth Science and Technology (JAMSTEC), Institute of Industrial Science, National Institute for Environmental Studies (NIES), Japan	Tachiiri et al. (2019)
MPI-ESM-1–2-HAM	250 km	Eidgenössische Technische Hochschule (ETH) Zürich, Switzerland, Leibniz Institute for Tropospheric Research, Germany, Max-Planck-Institut fuer Meteorologie, Germany, Federal Office of Meteorology and Climatology MeteoSwiss, Switzerland, Universität Bremen, Germany, Finnish Meteorological Institute, Finland, University of Exeter, Great Britain, Vrije Universiteit Amsterdam, Netherlands, University of Oxford, Great Britain	Neubauer et al. (2019)
MPI-ESM1-2-LR	250 km	Max-Planck-Institut fuer Meteorologie, Germany	Wieners et al. (2019)
MRI-ESM2-0	100 km	Meteorological Research Institute, Tsukuba, Japan	Yukimoto et al. (2019)

Table 9 List of CMIP6 models used in this study and their numbers corresponding those used in Figs. 2, 6, 7, 10, 11

Model number	Model name	Model number	Model name
1	BCC-ESM1-historical-r2i1p1f1	51	GISS-E2-1-H-historical-r2i1p5f1
2	BCC-ESM1-historical-r3i1p1f1	52	GISS-E2-1-H-historical-r3i1p1f1
3	CanESM5-CanOE-historical-r1i1p2f1	53	GISS-E2-1-H-historical-r3i1p1f2
4	CanESM5-historical-r11i1p1f1	54	GISS-E2-1-H-historical-r3i1p3f1
5	ACCESS-CM2-historical-r1i1p1f1	55	GISS-E2-1-H-historical-r3i1p5f1
6	ACCESS-CM2-historical-r2i1p1f1	56	GISS-E2-1-H-historical-r4i1p1f1
7	GFDL-CM4-historical-r1i1p1f1	57	GISS-E2-1-H-historical-r4i1p1f2
8	GISS-E2-1-G-CC-historical-r1i1p1f1	58	GISS-E2-1-H-historical-r4i1p3f1
9	GISS-E2-1-G-historical-r101i1p1f1	59	GISS-E2-1-H-historical-r5i1p1f1
10	GISS-E2-1-G-historical-r102i1p1f1	60	GISS-E2-1-H-historical-r5i1p1f2
11	GISS-E2-1-G-historical-r10i1p1f1	61	GISS-E2-1-H-historical-r6i1p1f1
12	GISS-E2-1-G-historical-r10i1p1f2	62	GISS-E2-1-H-historical-r7i1p1f1
13	GISS-E2-1-G-historical-r10i1p3f1	63	GISS-E2-1-H-historical-r8i1p1f1
14	GISS-E2-1-G-historical-r1i1p1f1	64	GISS-E2-1-H-historical-r9i1p1f1
15	CanESM5-historical-r1i1p2f1	65	ACCESS-ESM1-5-historical-r3i1p1f1
16	GISS-E2-1-G-historical-r1i1p1f2	66	MIROC6-historical-r10i1p1f1
17	GISS-E2-1-G-historical-r1i1p3f1	67	MIROC6-historical-r1i1p1f1
18	ACCESS-ESM1-5-historical-r1i1p1f1	68	MIROC6-historical-r3i1p1f1
19	GISS-E2-1-G-historical-r2i1p1f1	69	MIROC6-historical-r4i1p1f1
20	GISS-E2-1-G-historical-r2i1p1f2	70	MIROC6-historical-r5i1p1f1
21	GISS-E2-1-G-historical-r2i1p3f1	71	MIROC6-historical-r6i1p1f1
22	GISS-E2-1-G-historical-r3i1p1f1	72	MIROC6-historical-r7i1p1f1
23	GISS-E2-1-G-historical-r3i1p1f2	73	MIROC6-historical-r8i1p1f1
24	GISS-E2-1-G-historical-r4i1p1f1	74	MIROC6-historical-r9i1p1f1
25	GISS-E2-1-G-historical-r4i1p1f2	75	MIROC-ES2L-historical-r1i1p1f2
26	GISS-E2-1-G-historical-r5i1p1f1	76	MIROC-ES2L-historical-r2i1p1f2
27	GISS-E2-1-G-historical-r5i1p1f2	77	MIROC-ES2L-historical-r3i1p1f2
28	GISS-E2-1-G-historical-r5i1p3f1	78	MPI-ESM-1–2-HAM-historical-r1i1p1f1
29	GISS-E2-1-G-historical-r6i1p1f1	79	BCC-CSM2-MR-historical-r1i1p1f1
30	GISS-E2-1-G-historical-r6i1p1f2	80	MPI-ESM-1–2-HAM-historical-r2i1p1f1
31	GISS-E2-1-G-historical-r6i1p3f1	81	BCC-CSM2-MR-historical-r2i1p1f1
32	CanESM5-historical-r23i1p1f1	82	MPI-ESM1-2-LR-historical-r10i1p1f1
33	GISS-E2-1-G-historical-r7i1p1f2	83	MPI-ESM1-2-LR-historical-r1i1p1f1
34	GISS-E2-1-G-historical-r7i1p3f1	84	MPI-ESM1-2-LR-historical-r2i1p1f1
35	GISS-E2-1-G-historical-r8i1p1f1	85	MPI-ESM1-2-LR-historical-r3i1p1f1
36	GISS-E2-1-G-historical-r8i1p1f2	86	MPI-ESM1-2-LR-historical-r4i1p1f1
37	GISS-E2-1-G-historical-r8i1p3f1	87	MPI-ESM1-2-LR-historical-r5i1p1f1
38	GISS-E2-1-G-historical-r9i1p1f1	88	MPI-ESM1-2-LR-historical-r6i1p1f1
39	GISS-E2-1-G-historical-r9i1p1f2	89	MPI-ESM1-2-LR-historical-r7i1p1f1
40	GISS-E2-1-G-historical-r9i1p3f1	90	MPI-ESM1-2-LR-historical-r8i1p1f1
41	GISS-E2-1-H-historical-r10i1p1f1	91	MPI-ESM1-2-LR-historical-r9i1p1f1
42	ACCESS-ESM1-5-historical-r2i1p1f1	92	BCC-CSM2-MR-historical-r3i1p1f1
43	GISS-E2-1-H-historical-r1i1p1f1	93	MRI-ESM2-0-historical-r1i1p1f1
44	GISS-E2-1-H-historical-r1i1p1f2	94	MRI-ESM2-0-historical-r1i2p1f1
45	GISS-E2-1-H-historical-r1i1p3f1	95	MRI-ESM2-0-historical-r2i1p1f1
46	GISS-E2-1-H-historical-r1i1p5f1	96	MRI-ESM2-0-historical-r3i1p1f1
47	GISS-E2-1-H-historical-r2i1p1f1	97	MRI-ESM2-0-historical-r4i1p1f1

Table 9 (continued)

Model number	Model name	Model number	Model name
48	CanESM5-historical-r2i1p1f1	98	MRI-ESM2-0-historical-r5i1p1f1
49	GISS-E2-1-H-historical-r2i1p1f2	99	BCC-ESM1-historical-r1i1p1f1
50	GISS-E2-1-H-historical-r2i1p3f1	100	Mean of all 99 models

Abbreviations

AAM: Atmospheric angular momentum; AOD: Atmosphere and ocean dealiasing; AOD1B RL06: Atmosphere and Ocean Dealiasing Level-1b Release 6; CMIP: Coupled Model Intercomparison Project; CMIP6: Coupled Model Intercomparison Project Phase 6; CSR: Center for Space Research; EAM: Effective angular momentum; ECCO: Estimating the circulation and climate of the ocean; EOP: Earth orientation parameters; ECMWF: European Centre for Medium-Range Weather Forecasts; GAM: Geodetic angular momentum; GAO: Geodetic residuals: GAM–AAM–OAM; GFZ: GeoForschungsZentrum (eng. German Research Centre for Geosciences); GIA: Glacial isostatic adjustment; GLDAS: Global Land Data Assimilation System; GNSS: Global Navigation Satellite System; GRACE: Gravity Recovery and Climate Experiment; GRACE-FO: Gravity Recovery and Climate Experiment Follow-On; HAM: Hydrological angular momentum; IERS: International Earth Rotation and Reference System Service; JPL: Jet Propulsion Laboratory; LSDM: Land Surface Discharge Model; MPIOM: Max Planck Institute Ocean Model; NASA: National Aeronautics and Space Administration; NCEP/NCAR: National Centers for Environmental Prediction/National Center for Atmospheric Research; OAM: Atmospheric angular momentum; PM: Polar motion; RL: Release; SH: Spherical harmonics; SLR: Satellite laser ranging; TWS: Terrestrial water storage; VLBI: Very long baseline interferometry.

Acknowledgements

We kindly acknowledge: Christian Bizouard from Paris Observatory for providing GAM series computed from precise pole coordinates, the CSR team for providing GRACE Level-3 data, GFZ team for providing LSDM-based HAM series, all CMIP6 collaborators who provided climate models. All these datasets are publicly available for the users.

Author contributions

JN designed the study and performed HAM and GAO analyses. JŚ participated in HAM and GAO analyses and wrote the manuscript, with inputs of JN, TK, MW and AP. TK wrote the scripts for data analyses and prepared figures. All authors read and approved the final manuscript.

Funding

This research was funded by the National Science Center, Poland (NCN), Grant Number 2018/31/N/ST10/00209.

Availability of data and materials

CMIP6 models have been derived from the following website: https://esgf-data.dkrz.de/search/cmip6-dkrz/. GRACE CSR RL06 solution in the form of TWS anomalies (Level-3 data) has been obtained from NASA PO.DAAC Drive (https://podaac-tools.jpl.nasa.gov/drive/files/GeodeticsGravity/grace/L3). HAM series obtained from LSDM have been accessed from the GFZ website (http://esmdata.gfz-potsdam.de:8080/repository). GAM series have been computed from pole coordinates based on the EOP 14 C04 solution provided by IERS (https://www.iers.org/IERS/EN/DataProducts/EarthOrientationData/eop.html). AAM series based on ECMWF and OAM series based on MPIOM have been obtained from the GFZ website (http://esmdata.gfz-potsdam.de:8080/repository). OAM series based on ECCO model have been obtained from the IERS Special Bureau for the Oceans (https://www.iers.org/IERS/EN/DataProducts/GeophysicalFluidsData/geoFluids.html). AAM series based on NCEP/NCAR model have been obtained from the IERS Special Bureau for the Atmosphere (https://www.iers.org/IERS/EN/DataProducts/GeophysicalFluidsData/geoFluids.html). The data that support the findings of this study are available upon request from the corresponding author.

Declarations

Ethics approval and consent to participate

Not applicable.

Consent for publication

Not applicable.

Competing interests

The authors declare no conflict of interests.

Author details

[1]Centrum Badań Kosmicznych Polskiej Akademii Nauk, Bartycka 18A, 00-716 Warsaw, Poland. [2]Faculty of Civil Engineering, Warsaw University of Technology, Armii Ludowej 16, 00-637 Warsaw, Poland.

Received: 31 December 2021 Accepted: 26 April 2022
Published online: 02 June 2022

References

Adcroft A, Anderson W, Balaji V et al (2019) The GFDL global ocean and sea ice model OM4.0: model description and simulation features. J Adv Model Earth Syst 11:3167–3211. https://doi.org/10.1029/2019MS001726

Alsdorf DE, Lettenmaier DP (2003) Tracking fresh water from space. Science 301:1491–1494

Barnes RTH, Hide R, White AA, Wilson CA (1983) atmospheric angular momentum fluctuations, length-of-day changes and polar motion. Proc R Soc Lond Ser A Math Phys Sci 387:1792. https://doi.org/10.1098/rspa.1983.0050

Bettadpur S (2018) UTCSR Level–2 processing standards document for Level–2 Product Release 0006. Technical Report GRACE 2018. http://icgem.gfz-potsdam.de/GRACE_CSR_L2_Processing_Standards_Document_for_RL06.pdf

Brzeziński A (1992) Polar motion excitation by variations of the effective angular momentum function: considerations concerning deconvolution problem. Manuscr Geod 17:3–20

Brzeziński A, Nastula J, Kołaczek B (2009) Seasonal excitation of polar motion estimated from recent geophysical models and observations. J Geodyn 48(3–5):235–240. https://doi.org/10.1016/J.JOG.2009.09.021

Chao BF, Au AY (1991) Atmospheric excitation of the earth's annual wobble: 1980–1988. J Geophys Res 96(B4):6577–6582. https://doi.org/10.1029/91jb00041

Chen J (2019) Satellite gravimetry and mass transport in the earth system. Geod Geodyn 10:402–415. https://doi.org/10.1016/J.GEOG.2018.07.001

Chen JL, Wilson CR (2005) Hydrological excitations of polar motion, 1993–2002. Geophys J Int 160(3):833–839. https://doi.org/10.1111/j.1365-246X.2005.02522.x

Chen JL, Wilson CR, Chao BF et al (2000) Hydrological and oceanic excitations to polar motion and length-of-day variation. Geophys J Int 141:149–156. https://doi.org/10.1046/j.1365-246X.2000.00069.x

Chen J, Tapley B, Tamisiea ME et al (2021) Error assessment of GRACE and GRACE follow-on mass change. J Geophys Res Solid Earth 126:e2021JB022124. https://doi.org/10.1029/2021JB022124

Chen J, Cazenave A, Dahle C et al (2022) Applications and challenges of GRACE and GRACE follow-on satellite gravimetry. Surv Geophys. https://doi.org/10.1007/s10712-021-09685-x

Dickey JO, Marcus SL, Johns CM et al (1993) The oceanic contribution to the earth's seasonal angular momentum budget. Geophys Res Lett 20(24):2953–2956. https://doi.org/10.1029/93GL03186

Dill R (2008) Hydrological model LSDM for operational earth rotation and gravity field variations. Potsdam, GFZ German Research Centre for Geosciences. https://doi.org/10.2312/GFZ.b103-08095

Dill R, Thomas M, Walter C (2009) Hydrological induced earth rotation variations from stand-alone and dynamically coupled simulations. In: Soffel M, Capitaine N (eds) Proceedings of the journées 2008 systèmes de référence spatio-temporels. Lohrmann-Observatorium and Observatoire de, Paris, pp 115–118

Dobslaw H, Dill R, Grötzsch A et al (2010) Seasonal polar motion excitation from numerical models of atmosphere, ocean, and continental hydrosphere. J Geophys Res Solid Earth 115(10):1–11. https://doi.org/10.1029/2009JB007127

Eubanks TM (1993) Variations in the orientation of the earth. In: Smith DE, Turcotte DL (eds) Contributions of space geodesy to geodynamics: earth dynamics geodynamics series, vol 24. AGU, Washington, pp 1–54

Eyring V, Bony S, Meehl GA et al (2016) Overview of the coupled model intercomparison project phase 6 (CMIP6) experimental design and organization. Geosci Model Dev 9(5):1937–1958. https://doi.org/10.5194/gmd-9-1937-2016

Fukumori I, Wang O, Fenty I, et al (2017) ECCO Version 4 Release 3. http://hdl.handle.net/1721.1/110380 or https://dspace.mit.edu/handle/1721.1/110380.

Göttl F, Schmidt M, Seitz F, Bloßfeld M (2015) Separation of atmospheric, oceanic and hydrological polar motion excitation mechanisms based on a combination of geometric and gravimetric space observations. J Geod 89:377–390. https://doi.org/10.1007/s00190-014-0782-0

Göttl F, Schmidt M, Seitz F (2018) Mass-related excitation of polar motion: an assessment of the new RL06 GRACE gravity field models. Earth Planets Sp 70:195. https://doi.org/10.1186/s40623-018-0968-4

Gross RS (2003) Atmospheric and oceanic excitation of the earth's wobbles during 1980–2000. J Geophys Res 108(B8):6577–6582. https://doi.org/10.1029/2002jb002143

Gross RS (2007) Earth rotation variations—long period. In: Schubert G (ed) Treatise on geophysics. Elsevier, Amsterdam, pp 239–294. https://doi.org/10.1016/B978-044452748-6.00057-2

Gross RS (2015) Theory of earth rotation variations. In: Sneeuw N, Novák P, Crespi M, Sansò F (eds) VIII Hotine–Marussi symposium on mathematical geodesy, vol 142. Springer, Cham, pp 41–46

Hirst T, Bi D, Yan H, Marsland S, Dix M, Sullivan A (2015). The ACCESS-CM2 coupled climate model—status and plans including contribution to CMIP6. In: Greenhouse 2015, 27–30 October, Hobart. CSIRO. http://hdl.handle.net/102.100.100/91600?index=1

Jin S, Chambers DP, Tapley BD (2010) Hydrological and oceanic effects on polar motion from GRACE and models. J Geophys Res Solid Earth. https://doi.org/10.1029/2009JB006635

Jungclaus JH, Fischer N, Haak H et al (2013) Characteristics of the ocean simulations in the Max Planck institute ocean model (MPIOM) the ocean component of the MPI-earth system model. J Adv Model Earth Syst 5(2):422–446. https://doi.org/10.1002/jame.20023

Kalnay E, Kanamitsu M, Kistler R et al (1996) The NCEP/NCAR 40-year reanalysis project. Bull Am Meteorol Soc 77(3):437–472. https://doi.org/10.1175/1520-0477(1996)077%3c0437:TNYRP%3e2.0.CO;2

Kelley M, Schmidt GA, Nazarenko LS et al (2020) GISS-E2.1: configurations and climatology. J Adv Model Earth Syst 12:e2019MS002025. https://doi.org/10.1029/2019MS002025

Landerer FW, Flechtner FM, Save H et al (2020) Extending the global mass change data record: GRACE follow-on instrument and science data performance. Geophys Res Lett 47:e2020GL088306. https://doi.org/10.1029/2020GL088306

Lettenmaier DP, Famiglietti JS (2006) Hydrology: water from on high. Nature 444:562–563

Meyrath T, van Dam T (2016) A comparison of interannual hydrological polar motion excitation from GRACE and geodetic observations. J Geodyn 99:1–9. https://doi.org/10.1016/J.JOG.2016.03.011

Munk WH, MacDonald G (1960) The rotation of the Earth. Cambridge University Press, Cambridge, UK

NASA Goddard institute for space studies (NASA/GISS) (2019). NASA-GISS GISS-E2–1-G-CC model output prepared for CMIP6 CMIP historical. Version YYYYMMDD. Earth System Grid Federation. https://doi.org/10.22033/ESGF/CMIP6.11762

Nastula J, Śliwińska J (2020) Prograde and retrograde terms of gravimetric polar motion excitation estimates from the GRACE monthly gravity field models. Remote Sens 12(1):138. https://doi.org/10.3390/rs12010138

Nastula J, Paśnicka M, Kołaczek B (2011) Comparison of the geophysical excitations of polar motion from the period: 1980.0–2009.0. Acta Geophys 59(3):561–577. https://doi.org/10.2478/s11600-011-0008-2

Nastula J, Wińska M, Śliwińska J, Salstein D (2019) Hydrological signals in polar motion excitation—evidence after fifteen years of the GRACE mission. J Geodyn 124:119–132. https://doi.org/10.1016/j.jog.2019.01.014

Neubauer D, Ferrachat S, Siegenthaler-Le Drian C, et al (2019) HAMMOZ-Consortium MPI-ESM1.2-HAM model output prepared for CMIP6 AerChemMIP. Version 2019. Earth System Grid Federation. https://doi.org/10.22033/ESGF/CMIP6.1621

Njoku EG, Jackson TJ, Lakshmi V et al (2003) Soil moisture retrieval from AMSR-E. IEEE Trans Geosci Remote Sens 41:215–229. https://doi.org/10.1109/TGRS.2002.808243

Ponte RM, Stammer D, Marshall J (1998) Oceanic signals in observed motions of the earth's pole of rotation. Nature 391:476–479. https://doi.org/10.1038/35126

Seoane L, Nastula J, Bizouard C, Gambis D (2009) The use of gravimetric data from GRACE mission in the understanding of polar motion variations. Geophys J Int 178:614–622. https://doi.org/10.1111/j.1365-246X.2009.04181.x

Seoane L, Nastula J, Bizouard C, Gambis D (2011) Hydrological excitation of polar motion derived from GRACE gravity field solutions. Int J Geophys. https://doi.org/10.1155/2011/174396

Seoane L, Biancale R, Gambis D (2012) Agreement between earth's rotation and mass displacement as detected by GRACE. J Geodyn 62:49–55. https://doi.org/10.1016/j.jog.2012.02.008

Shiogama H, Abe M, Tatebe H (2019) MIROC MIROC6 model output prepared for CMIP6 ScenarioMIP. Version YYYYMMDD. Earth System Grid Federation. https://doi.org/10.22033/ESGF/CMIP6.898

Śliwińska J, Wińska M, Nastula J (2019) Terrestrial water storage variations and their effect on polar motion. Acta Geophys 67:17–39. https://doi.org/10.1007/s11600-018-0227-x

Śliwińska J, Nastula J, Dobslaw H, Dill R (2020a) Evaluating gravimetric polar motion excitation estimates from the RL06 GRACE monthly-mean gravity field models. Remote Sens 12(6):930. https://doi.org/10.3390/rs12060930

Śliwińska J, Wińska M, Nastula J (2020b) Preliminary estimation and validation of polar motion excitation from different types of the GRACE and GRACE Follow-on missions data. Remote Sens 12(21):3490. https://doi.org/10.3390/rs12213490

Śliwińska J, Nastula J, Wińska M (2021a) Evaluation of hydrological and cryospheric angular momentum estimates based on GRACE, GRACE-FO and SLR data for their contributions to polar motion excitation. Earth Planets Sp 73:71. https://doi.org/10.1186/s40623-021-01393-5

Śliwińska J, Wińska M, Nastula J (2021b) Validation of GRACE and GRACE-FO mascon data for the study of polar motion excitation. Remote Sens 13(6):1152. https://doi.org/10.3390/rs13061152

Swart NC, Cole JNS, Kharin VV et al (2019) The Canadian earth system model version 5 (CanESM5.0.3). Geosci Model Dev. https://doi.org/10.5194/gmd-12-4823-2019

Tachiiri K, Abe M, Hajima T, et al (2019) MIROC MIROC-ES2L model output prepared for CMIP6 ScenarioMIP. Version YYYYMMDD. Earth System Grid Federation. https://doi.org/10.22033/ESGF/CMIP6.936

Tapley BD, Bettadpur S, Watkins M, Reigber C (2004) The gravity recovery and climate experiment: Mission overview and early results. Geophys Res Lett 31(9):4. https://doi.org/10.1029/2004GL019920

Taylor KE, Stouffer RJ, Meehl GA (2012) An overview of CMIP5 and the experiment design. Bull Am Meteorol Soc 93(4):485–498. https://doi.org/10.1175/BAMS-D-11-00094.1

Taylor KE, Juckes M, Balaji V, et al (2018). CMIP6 Global Attributes, DRS, Filenames, Directory Structure, and CV's. Available online: https://goo.gl/v1drZl

Vicente RO, Wilson CR (2002) On long-period polar motion. J Geod 76:199–208. https://doi.org/10.1007/s00190-001-0241-6

Wahr JM (1983) The effects of the atmosphere and oceans on the earth's wobble and on the seasonal variations in the length of day—II. results. Geophys J R Astron Soc 74(2):451–487. https://doi.org/10.1111/j.1365-246X.1983.tb01885.x
Wahr J, Swenson S, Zlotnicki V, Velicogna I (2004) Time-variable gravity from GRACE: first results. Geophys Res Lett. https://doi.org/10.1029/2004GL019779
Wieners K-H, Giorgetta M, Jungclaus J, et al (2019) MPI-M MPI-ESM1.2-LR model output prepared for CMIP6 ScenarioMIP ssp245. Version YYYYMMDD. Earth System Grid Federation. https://doi.org/10.22033/ESGF/CMIP6.6693
Wińska M (2016) Hydrological excitations of polar motion derived from different variables of Fgoals—G 2 climate model. Artif Satell 51(4):107–122. https://doi.org/10.1515/arsa-2016-0010
Wińska M, Śliwińska J (2019) Assessing hydrological signal in polar motion from observations and geophysical models. Stud Geophys Geod 63:95–117. https://doi.org/10.1007/s11200-018-1028-z
Wińska M, Nastula J, Kołaczek B (2016) Assessment of the global and regional land hydrosphere and its impact on the balance of the geophysical excitation function of polar motion. Acta Geophys 64:270–292. https://doi.org/10.1515/acgeo-2015-0041
Wińska M, Nastula J, Salstein D (2017) Hydrological excitation of polar motion by different variables from the GLDAS models. J Geod 91:1461–1473. https://doi.org/10.1007/s00190-017-1036-8
Wu T, Lu Y, Fang Y et al (2019) The beijing climate center climate system model (BCC-CSM): the main progress from CMIP5 to CMIP6. Geosci Model Dev 12:173–1600. https://doi.org/10.5194/gmd-12-1573-2019
Wu T, Fang Z, Jie Z et al (2020) Beijing climate center earth system model version 1 (BCC-ESM1): model description and evaluation of aerosol simulations. Geosci Model Dev 13:977–1005. https://doi.org/10.5194/gmd-13-977-2020
Yukimoto S, Koshiro T, Kawai H, et al (2019) MRI MRI-ESM20 model output prepared for CMIP6 CMIP. Earth System Grid Federation. https://doi.org/10.22033/ESGF/CMIP6.621
Ziehn T, Chamberlain M, Lenton A, et al (2019) CSIRO ACCESS-ESM1.5 model output prepared for CMIP6 CMIP. Earth System Grid Federation. https://doi.org/10.22033/ESGF/CMIP6.2288

Publisher's Note